Automatica 133 (2021) 109830

Contents lists available at ScienceDirect

Automatica

journal homepage: www.elsevier.com/locate/automatica

Projection-based integrators for improved motion control: Formalization, well-posedness and stability of hybrid integrator-gain systems ☆

Daniel Andreas Deenen [a], Bardia Sharif [a,*], Sebastiaan van den Eijnden [a], Hendrik Nijmeijer [a], Maurice Heemels [a], Marcel Heertjes [a,b]

[a] Department of Mechanical Engineering, Eindhoven University of Technology, 5600 MB, Eindhoven, The Netherlands
[b] Mechatronics System Development, ASML, 5504 DR, Veldhoven, The Netherlands

ARTICLE INFO

Article history:
Received 29 November 2019
Received in revised form 23 April 2021
Accepted 16 June 2021
Available online 14 August 2021

ABSTRACT

In this paper we formally describe the hybrid integrator-gain system (HIGS), which is a nonlinear integrator designed to avoid the limitations typically associated with linear integrators. The HIGS keeps the sign of its input and output equal, thereby inducing less phase lag than a linear integrator, much like the famous Clegg integrator. The HIGS achieves the reduced phase lag by projection of the controller dynamics instead of using resets of the integrator state, which forms a potential benefit of this control element. To formally analyze HIGS-controlled systems, we present an appropriate mathematical framework for describing these novel systems. Based on this framework, HIGS-controlled systems are proven to be well-posed in the sense of existence and forward completeness of solutions. Moreover, we propose two approaches for analyzing (input-to-state) stability of the resulting nonlinear closed-loop systems: (i) circle-criterion-like conditions based on (measured) frequency response data, and (ii) LMI-based conditions exploiting a new construction of piecewise quadratic Lyapunov functions. A motion control example is used to illustrate the results.

1. Introduction

For the control of linear motion systems, linear time invariant (LTI) control theory is appealing due to its well-understood and straightforward controller design with guaranteed stability and performance properties. However, LTI control designs suffer from fundamental performance limitations such as Bode's gain-phase relationship and the waterbed effect due to Bode's sensitivity integral (Freudenberg, Middleton, & Stefanpoulou, 2000; Seron, Braslavsky, & Goodwin, 1997). In the context of closed-loop performance, this typically results in design trade-offs.

To overcome these fundamental limitations of LTI control, various hybrid and nonlinear control strategies for linear motion systems have been proposed, see, for example, Feuer, Goodwin, and Salgado (1997), Zheng, Chait, Hollot, Steinbuch, and Norg (2000) and the references therein. One particularly interesting solution is reset control (Aangenent, Witvoet, Heemels, van de Molengraft, & Steinbuch, 2009; Baños & Barreiro, 2012; Beker, Hollot, Chait, & Han, 2004; Chait & Hollot, 2002; Clegg, 1958; Hazeleger, Heertjes, & Nijmeijer, 2016; van Loon, Gruntjens, Heertjes, van de Wouw, & Heemels, 2017; Nešić, Zaccarian, & Teel, 2008; Prieur, Queinnec, Tarbouriech, & Zaccarian, 2018; Saikumar & Hosseinnia, 2017), which started with the introduction of the Clegg integrator (Clegg, 1958), being an integrator that resets its state to zero upon zero input crossings. The development of reset control continued with generalizations such as the first-order reset element (Beker et al., 2004; Chait & Hollot, 2002; Horowitz & Rosenbaum, 1975; Zhao, Nešić, Tan, & Hua, 2019), the second-order reset element (Hazeleger et al., 2016) and generalized fractional order reset elements (Saikumar & Hosseinnia, 2017). Extensive research on reset control systems has led to various fruitful results regarding stability analysis (Barreiro & Baños, 2010; Beker et al., 2004; Carrasco & Navarro-López, 2013; Guo, Wang, Xie, & Zheng, 2009; Nešić, Teel, & Zaccarian, 2011; Nešić

☆ This work is partly carried out under the project "From PID to complex order controller (CLOC)" supported by the Netherlands Organization for Scientific Research (NWO) Domain for Applied and Engineering Sciences (TTW), The Netherlands. The material in this paper was partially presented at: [1.] the 2017 American Control Conference, May 24–26, 2017, Seattle, WA, USA. [2.] The 58th IEEE Conference on Decision and Control, December 11–13, 2019, Nice, France. This paper was recommended for publication in revised form by Associate Editor Luca Zaccarian under the direction of Editor Daniel Liberzon.

* Corresponding author.
E-mail addresses: d.a.deenen@tue.nl (D.A. Deenen), b.sharif@tue.nl (B. Sharif), s.j.a.m.v.d.eijnden@tue.nl (S. van den Eijnden), h.nijmeijer@tue.nl (H. Nijmeijer), m.heemels@tue.nl (M. Heemels), M.F.Heertjes@tue.nl (M. Heertjes).

https://doi.org/10.1016/j.automatica.2021.109830

et al., 2008; Zaccarian, Nešić, & Teel, 2011), beating fundamental time-domain performance limitations of LTI control (Beker, Hollot, & Chait, 2001; Zhao et al., 2019), hybrid formulations (Zaccarian, Nešić, & Teel, 2005) using temporal regularization to avoid Zeno phenomena, and experimental demonstration of reset control systems achieving improved performance (Baños, Perez, & Cervera, 2013; Hazeleger et al., 2016; Saikumar & Hosseinnia, 2017; Vidal & Banos, 2008). A desirable feature typical of reset controllers is characterized by the Clegg integrator's describing function, which exhibits a 20 dB/decade amplitude decay similar to that of a linear integrator, however induces only 38.15 degrees of phase lag (as opposed to 90 degrees for the linear integrator). The latter is a result of the reset forcing the integrator's input and output to always be of equal sign. This is a general feature of many reset controllers, in which the resetting mechanism leads to an improvement in phase lag over its linear counterpart, which in turn suggests the possibility of designing a compensator capable of supplying the required bandwidth with a much reduced gain at high frequencies (Chait & Hollot, 2002). Clearly, this favorable phase behavior can significantly improve closed-loop performance.

Inspired by the advantages of reset control, in this paper we are interested in formalizing, as an alternative to reset control, a new nonlinear integrator referred to as the hybrid integrator-gain system (HIGS), which offers the same phase advantages, but without the need for hard resets of the (integrator) state.

The HIGS is designed to keep its input–output relation bounded in the sector $[0, k_h]$, where $k_h \in \mathbb{R}_{>0}$ denotes the gain parameter, thereby inheriting the hinted phase advantage of reset control (as the input and output of the HIGS have the same sign). However, the HIGS avoids resetting the integrator state, and exploits *projection* of the (controller) dynamics in a manner resulting in continuous control signals. In particular, a HIGS element acts as a linear integrator as long as its input–output pair lies inside the mentioned sector (called the 'integrator mode'). At moments when the sector condition tends to be violated, the vector field of the HIGS element is altered via projection in such a way that the resulting trajectories stay on the boundary of the sector. This second mode of operation is referred to as the 'gain mode' of the HIGS, explaining the terminology of hybrid integrator-gain systems. Interestingly, upon switching from integrator to gain mode, the integrator buffer is preserved as much as possible while respecting the sector condition, instead of being completely depleted by resets. This leads to increased potential for improving closed-loop performance for this hybrid integrator in comparison to, for instance, the Clegg integrator.

In this paper, we formalize the above idea based on extensions of so-called projected dynamical systems (PDS) (Dupuis & Nagurney, 1993; Henry, 1973; Nagurney & Zhang, 2012), a class of discontinuous dynamical systems introduced in the early 1990s. PDS are described by differential equations of which the solutions are restricted to a constraint set. At moments when the solutions tend to leave this set, the vector field of the system is changed by means of projection so that the solutions remain inside the constraint set. Although the PDS philosophy resembles that of the HIGS, there are essential differences that prevent direct description of the HIGS as a PDS. First of all, the constraint set of the HIGS (the sector), does not satisfy the regularity requirements that the PDS framework commonly requires, see, e.g., Henry (1973). Secondly, in the case of PDSs, the complete vector field is projected on (the tangent cone of) the constraint set. In the context of control, however, when considering a HIGS element in feedback interconnection with a physical plant, it is only possible to project the dynamics of the controller (HIGS) and not the full dynamics (including the plant dynamics). This calls for important generalizations of PDS, as provided in this paper, for which we coin the term *extended projected dynamical systems* (ePDS). Based on this new ePDS framework, which naturally captures the design philosophy of HIGS, we provide a formal mathematical description of HIGS-controlled systems. Interestingly, the representation used in our preliminary work (Deenen, Heertjes, Heemels, & Nijmeijer, 2017) follows from the ePDS-based formulation of HIGS-controlled systems. Furthermore, we establish the well-posedness of HIGS-controlled systems in the sense of existence and forward completeness of solutions, under mild assumptions as generally satisfied for linear motion systems.

In our preliminary work (Deenen et al., 2017), a circle-criterion-like argument is presented for stability analysis of HIGS-controlled systems (however, without a proof of the stability and without a well-posedness proof). Clearly, this circle-criterion approach offers great advantages in terms of easy-to-check graphical conditions based on accurate and quickly measurable frequency response functions. A potential drawback, however, is that it may yield conservative bounds on closed-loop stability due to (i) the underlying use of a *common* quadratic Lyapunov function for a piecewise linear closed-loop system (Sontag, 1981), and (ii) solely using the hybrid integrator's sector-boundedness instead of its complete nonlinear dynamic behavior. Furthermore, its application is limited to control configurations where a *stable* LTI system is used in feedback connection with a HIGS element. One of the key contributions of this paper, next to providing a full proof of the circle-criterion-like stability condition for the first time, is to also provide less conservative stability conditions in terms of linear matrix inequalities (LMIs). This approach is inspired by Aangenent et al. (2009) and Zaccarian et al. (2005, 2011) for reset control systems, where LMIs guarantee stability based on a *piecewise* quadratic (PWQ) Lyapunov function by partitioning the two-dimensional input–output plane of the reset element into double cones with the apices at the origin. The HIGS differs from the previously considered reset integrators in the sense that its switching dynamics are determined in a *three-dimensional* space. Therefore, an extension of the planar approach is proposed that uses volumetric partitions in a spherical coordinate system leading to LMI-based (input-to-state) stability conditions for HIGS-controlled systems. Both methods will be used to verify stability of an LTI motion system in feedback with a HIGS to illustrate, on the one hand, the practical convenience of the circle-criterion-like approach, and, on the other hand, the increased potential of the LMI-based conditions in terms of reduced conservativeness regarding parameter bounds.

The remainder of this paper is organized as follows. Section 2 contains preliminaries and notation. The HIGS is described in Section 3 and proven to be well-posed in Section 4. In Section 5, the LMI-based closed-loop stability conditions and their derivation are discussed, followed by the circle-criterion-like frequency-domain stability conditions in Section 6. In Section 7, these stability conditions are compared using an illustrative motion control example. Section 8 states the conclusions.

2. Definitions and preliminaries

A sequence of real scalars $(u^1, u^2, \ldots, u^k)$ with $k \in \mathbb{N}$ and $u^l \in \mathbb{R}$, $l = 1, 2, \ldots, k$, is called lexicographically non-negative (non-positive), written as $(u^1, u^2, \ldots, u^k) \geq_l 0$ ($\leq_l 0$), if $(u^1, u^2, \ldots, u^k) = (0, 0, \ldots, 0)$ or $u^j > 0$ (< 0) where $j = \min\{l \in \{1, \ldots, k\} \mid u^l \neq 0\}$. For the column space (image) and the null-space (kernel) of a matrix $H \in \mathbb{R}^{n\times m}$ we write $\mathrm{im}H = \{Hx \mid x \in \mathbb{R}^m\}$ and $\ker H := \{x \in \mathbb{R}^m \mid Hx = 0\}$.

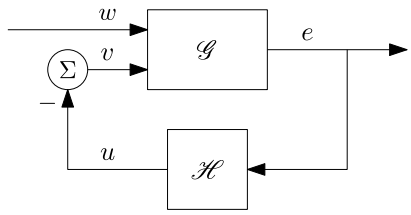

Fig. 1. Closed-loop system in Lur'e form.

Definition 2.1. A function $w : \mathcal{I} \to \mathbb{R}^{n_w}$, with $\mathcal{I} \subseteq \mathbb{R}$ is called a Bohl function, denoted by $w \in B_{\mathcal{I}}$, if there exist matrices $H \in \mathbb{R}^{n_w \times n_F}$, $F \in \mathbb{R}^{n_F \times n_F}$, and a vector $v \in \mathbb{R}^{n_F}$ such that $w(t) = He^{Ft}v$ for all $t \in \mathcal{I}$.

Definition 2.2. A function $w : \mathbb{R}_{\geq 0} \to \mathbb{R}^{n_w}$ is called a piecewise Bohl function, denoted by $w \in PB$, if there exists a sequence $\{t_i\}_{i\in\mathbb{N}}$ with $0 = t_0 < t_i < t_{i+1}$ for all $i \in \mathbb{N}$ and $t_i \to \infty$ when $i \to \infty$ such that $w : [t_i, t_{i+1}) \to \mathbb{R}^{n_w}$ is a Bohl function for each $i \in \mathbb{N}$.

Note that piecewise Bohl functions can be discontinuous, but they are continuous from the right in the sense that for each $T \in \mathbb{R}_{\geq 0}$ it holds that $w(T) = \lim_{t\downarrow T} w(t)$.

Definition 2.3. An absolutely continuous (AC) function $f : [a, b] \to \mathbb{R}^n$ is a function that can be written as $f(t) - f(a) = \int_a^t \dot{f}(\tau)d\tau$ for any $t \in [a, b]$ for a Lebesgue integrable function $\dot{f} \in \mathcal{L}^1([a, b], \mathbb{R}^n)$, which is considered as its derivative. A function $f : \mathcal{I} \to \mathbb{R}^n$ is locally AC, if it is AC for any bounded interval $[a, b] \subset \mathcal{I}$.

Definition 2.4 (*Rockafellar & Wets, 1998*)**.** The tangent cone to a set $S \subset \mathbb{R}^n$ at a point $\xi \in S$, denoted by $T_S(\xi)$, is the set of all vectors $v \in \mathbb{R}^n$ for which there exist sequences $\{\xi_i\}_{i\in\mathbb{N}} \in S$ and $\{\tau_i\}_{i\in\mathbb{N}}$, $\tau_i > 0$, $i \in \mathbb{N}$, with $\xi_i \to \xi$, $\tau_i \downarrow 0$ and $i \to \infty$, such that $v = \lim_{i\to\infty} \frac{\xi_i - \xi}{\tau_i}$.

3. System description

In this section we consider the closed-loop system setup in Fig. 1, consisting of a linear time-invariant (LTI), single-input single-output (SISO) plant $\mathcal{G}$ interconnected with a (SISO) HIGS element $\mathcal{H}$. The plant $\mathcal{G}$ contains the linear part of the closed-loop system including the plant to be controlled and possibly an LTI controller, given by the state–space representation

$$\mathcal{G} : \begin{cases} \dot{x}_g &= A_g x_g + B_{gv} v + B_{gw} w, \quad \text{(a)} \\ e &= C_g x_g, \quad \text{(b)} \end{cases} \tag{1}$$

with states x_g taking values in $\mathbb{R}^{n_g}$, performance output e in $\mathbb{R}$, control input v in $\mathbb{R}$ and exogenous disturbances and references denoted by w taking values in $\mathbb{R}^{n_w}$. Moreover, the realization (A_g, B_{gv}, C_g) is assumed to be minimal. As our key area of application involves motion systems containing floating masses, the following assumption is typically satisfied.

Assumption 3.1. The LTI system $\mathcal{G}$ as in Fig. 1 is such that $C_g B_{gw} = 0$ and $C_g B_{gv} = 0$.

The HIGS element $\mathcal{H}$ has as its preferred mode of operation the linear integrator dynamics

$$\begin{aligned} \dot{x}_h &= \omega_h e, \\ u &= x_h, \end{aligned} \tag{2}$$

where the state x_h takes values in $\mathbb{R}$, the (HIGS) input e and the (HIGS) output u both take values in $\mathbb{R}$ and $\omega_h \in [0, \infty)$ denotes the integrator frequency. This mode of operation of the HIGS is referred to as the *integrator mode*. The integrator mode (2) can only be used as long as the input–output pair (e, u) of $\mathcal{H}$ remains inside

$$\mathcal{F} := \left\{ (e, u) \in \mathbb{R}^2 \mid eu \geq \frac{1}{k_h} u^2 \right\}, \tag{3}$$

where $k_h \in (0, \infty)$ denotes the gain parameter of $\mathcal{H}$. Note that $(e, u) \in \mathcal{F}$ implies equal sign of the input e and the output u of the HIGS as $eu \geq 0$, see Fig. 2. At moments when the input–output pair (e, u) of $\mathcal{H}$ tends to leave the sector $\mathcal{F}$ we will "project" the integrator dynamics in (2) such that $(e, u) \in \mathcal{F}$ remains true along the trajectories of the system. We will formalize this operation of the HIGS in the upcoming subsections.

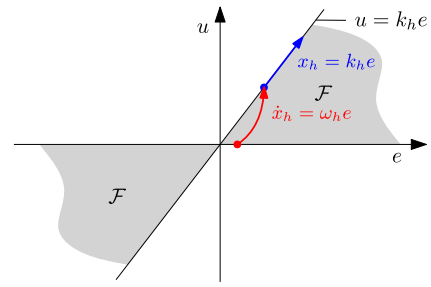

Fig. 2. An example of a HIGS in operation.

3.1. Projection-based representation

To mathematically introduce the operation of the HIGS, we directly use the interconnection of the HIGS element $\mathcal{H}$ and the linear system $\mathcal{G}$ described by (1), resulting in a closed-loop system as in Fig. 1, with state $x = \begin{bmatrix} x_g^\top & x_h^\top \end{bmatrix}^\top$ taking values in $\mathbb{R}^n$, where x_g and x_h are the states of $\mathcal{G}$ and $\mathcal{H}$, respectively and thus $n = n_g + 1$. Note that the constraint $(e, u) \in \mathcal{F}$ translates to $x \in \mathcal{S}$ with

$$\mathcal{S} = \mathcal{K} \cup -\mathcal{K}, \tag{4}$$

where $\mathcal{K}$ is a polyhedral cone given by

$$\mathcal{K} := \{x \in \mathbb{R}^n \mid Fx \geq 0\}, \tag{5}$$

where $F = \begin{bmatrix} F_1^\top & F_2^\top \end{bmatrix}^\top$ with $F_1 = \begin{bmatrix} k_h C_g & -1 \end{bmatrix}$, and $F_2 = \begin{bmatrix} 0_{n_g \times 1} & 1 \end{bmatrix}$. In fact, $F_1 x = k_h e - u$ and $F_2 x = u$ such that $(e, u) \in \mathcal{F}$ if and only if $x \in \mathcal{S}$. When $\mathcal{H}$ operates in the integrator mode, by combining (1) and (2) we obtain the state space representation for the HIGS-controlled system in Fig. 1, given by

$$\begin{aligned} \dot{x} &= A_1 x + Bw, \\ y &= Cx, \end{aligned} \tag{6}$$

where $y = [e \quad u]^\top$, and

$$\left[\begin{array}{c|c} A_1 & B \\ \hline C & \end{array}\right] = \left[\begin{array}{cc|c} A_g & -B_{gv} & B_{gw} \\ \omega_h C_g & 0 & 0_{1\times n_w} \\ \hline C_g & 0 & \\ 0_{1\times n_g} & 1 & \end{array}\right]. \tag{7}$$

As indicated above, when the state trajectory tends to leave the set $\mathcal{S}$, which in terms of Definition 2.4 happens when

$$A_1 x(t) + Bw(t) \notin T_{\mathcal{S}}(x(t)), \tag{8}$$

for $x(t) \in \mathcal{S}$, the vector field of (6), is altered by partial projection such that the resulting trajectory remains inside $\mathcal{S}$. Using this perspective, we can formally introduce the HIGS-controlled system

as

$$\Sigma := \begin{cases} \dot{x} = \Pi_{\mathcal{S},E}(x, A_1x + Bw), \\ y = Cx, \end{cases} \tag{9}$$

where for $x \in \mathcal{S}$ and $f \in \mathbb{R}^n$

$$\Pi_{\mathcal{S},E}(x, f) := \underset{\substack{a \in T_{\mathcal{S}(x)} \\ a - f \in \mathrm{im}E}}{\arg\min} \|a - f\| \tag{10}$$

with $\Pi_{\mathcal{S},E} : \mathcal{S} \times \mathbb{R}^n \to \mathbb{R}^n$ an operator, which projects the dynamics f onto the tangent cone of the set $\mathcal{S}$ at point x, in the direction im$E$. In the case of (9), $E = [0^\top_{n_p \times 1} \quad 1]^\top$ such that the correction of the dynamics (6) is only possible for the dynamics of the HIGS and not for the (physical) plant dynamics (1), which can clearly not be modified (we cannot directly modify $\dot{x}_g$). Note that the projection operator $\Pi_{\mathcal{S},E}$, is well-defined in the sense that it provides a unique outcome for every $x \in \mathcal{S}$ and each $f \in \mathbb{R}^n$, in the setting considered here (see Sharif, Heertjes, & Heemels, 2019).

The model (10) resembles so-called projected dynamical systems (PDS) (Henry, 1973; Nagurney & Zhang, 2012) given by

$$\dot{x}(t) = \Pi_{\mathcal{S}}(x(t), f(x(t))) = \underset{v \in T_{\mathcal{S}(x(t))}}{\arg\min} \|v - f(x(t))\|, \tag{11}$$

where $f : \mathbb{R}^n \to \mathbb{R}^n$ is a general vector field and $\mathcal{S} \subseteq \mathbb{R}^n$ is a constraint set. Our representation (10) differs from (11) in two essential ways. First of all, we have partial projection of dynamics as a result of using the matrix E, the image of which specifies the direction of projection. It should be noted that the matrix E is not limited to the choice made in (9) and should be chosen depending on the specific case under consideration. Secondly, in the PDS literature, the PDS (11) is shown to be well-defined for constraint sets that satisfy certain regularity conditions. In particular, Henry (1973) and Nagurney and Zhang (2012) restrict the constraint sets to be convex, while in Hauswirth, Bolognani, and Dorfler (2021) (and some references therein) convexity is relaxed to Clarke regularity and prox-regularity of the constraint set for existence and uniqueness of Carathéodory solutions, respectively. However, the constraint set $\mathcal{S}$ considered here does not satisfy any of the above mentioned regularity requirements, cf. (4). In addition, note that (10) is a generalization of (11) since by taking im$E = \mathbb{R}^n$ and restricting $\mathcal{S}$ to satisfy the required conditions, one recovers the classical PDS as in (11). In fact, for these reasons we refer to the class of systems (10) as extended projected dynamical systems (ePDS).

Remark 3.1. Note that we could extend the dynamics (9) that are currently defined for initial states $x(0) \in \mathcal{S}$, such that they are also defined for $x(0) \notin \mathcal{S}$. In case $x(0) \notin \mathcal{S}$, we can use $x(0^+) = \mathrm{argmin}_{s \in C_x} \|s - x\|$ with $C_x := \{s \in \mathcal{S} \mid s - x \in \mathrm{im}\, E\}$, to reset the state to a state inside $\mathcal{S}$. Note that this reset only occurs at the initial time and not afterwards, as the state never leaves $\mathcal{S}$ for time $t \in \mathbb{R}_{>0}$.

Remark 3.2. It is easy to see that (9) satisfies

$$\Pi_{\mathcal{S},E}(x, A_1x + Bw) = -\Pi_{\mathcal{S},E}(-x, -(A_1x + Bw)).$$

This symmetry property will prove to be useful in Section 4, in showing well-posedness of the system.

3.2. Discontinuous PWL model

In this subsection we reformulate (9) as an equivalent piecewise linear (PWL) model. To explicitly compute (9), we first note that

$$T_{\mathcal{S}}(x) = \begin{cases} T_{\mathcal{K}}(x), & \text{if } x \in \mathcal{K} \setminus -\mathcal{K}, \\ \mathcal{K} \cup -\mathcal{K}, & \text{if } x \in \mathcal{K} \cap -\mathcal{K}, \\ -T_{\mathcal{K}}(-x), & \text{if } x \in -\mathcal{K} \setminus \mathcal{K}, \end{cases} \tag{12}$$

where $T_{\mathcal{K}}(x) = \{a \in \mathbb{R}^n \mid F_{I(x)}a \geq 0\}$, with $I(x) = \{i \in \{1, 2\} \mid F_ix = 0\}$. Based on (7), (12), and Assumption 3.1, we obtain that $A_1x + Bw \in T_{\mathcal{S}}(x)$ if and only if $x \in \mathcal{S}_1$ with

$$\begin{aligned} \mathcal{S}_1 = \{x \in \mathbb{R}^n \mid F_2x \geq 0 \wedge (F_1x, F_1(A_1x)) \geq_l 0\} \cup \\ \{x \in \mathbb{R}^n \mid F_2x \leq 0 \wedge (F_1x, F_1(A_1x)) \leq_l 0\}. \end{aligned} \tag{13}$$

The proof of the statement above can be established by comparing the algebraic expressions of (12) and (13) for states lying in the interior of $\mathcal{S}$ where $F_1x > (<)0$ and $F_2x > (<)0$, and its boundaries where $F_1x = 0$ or $F_2x = 0$. Due to space limitations a complete proof is omitted here.

As a result of the discussion above, $\mathcal{S}_1$ is the region where the integrator mode of $\mathscr{H}$ is active. Moreover, when

$$\begin{aligned} x \in \mathcal{S}_2 &:= \{x \in \mathcal{S} \mid x \notin \mathcal{S}_1\} \\ &= \underbrace{\{x \in \mathcal{S} \mid F_2x \geq 0 \wedge F_1x = 0 \wedge F_1(A_1x) < 0\}}_{\mathcal{S}_2^+} \cup \\ &\underbrace{\{x \in S \mid F_2x \leq 0 \wedge F_1x = 0 \wedge F_1(A_1x) > 0\}}_{\mathcal{S}_2^-}, \end{aligned} \tag{14}$$

(8) holds. Based on (9) and (12) (with $f = A_1x + Bw$ and $\mathcal{S}$ as in (4)), when $x \in \mathcal{S}_2$, by solving (9), through manipulating (10) (see equation (17) in Sharif et al., 2019) and resorting to the Karush–Kuhn–Tucker (KKT) optimality conditions for constrained optimization (Boyd & Vandenberghe, 2004), we obtain

$$\begin{aligned} \dot{x} &= A_1x + Bw + E((F_1E)^{-1}(-F_1A_1x - F_1Bw)) \\ &= \underbrace{(I - E((F_1E)^{-1}F_1)(A_1x))}_{A_2x} + Bw =: A_2x + Bw. \end{aligned} \tag{15}$$

We refer to (15) as the gain mode dynamics. By considering both modes of operation (given by (6) and (15)) and their corresponding regions, we obtain the explicit *discontinuous* PWL model

$$\begin{aligned} \dot{x} &= \Pi_{\mathcal{S},E}(x, A_1x + Bw) = \begin{cases} A_1x + Bw, & \text{if } x \in \mathcal{S}_1, \\ A_2x + Bw, & \text{if } x \in \mathcal{S}_2, \end{cases} \\ y &= Cx \end{aligned} \tag{16}$$

for (9). Note that $\mathcal{S}_1$ has a non-empty interior while $\mathcal{S}_2$ does not (it is part of the lower-dimensional sub-space kerF_1). The matrices A_1, B and, C have been explicitly computed in (7). We can also compute A_2 from (15) as

$$\begin{aligned} \dot{x} &= A_1x + Bw + E((F_1E)^{-1}(-F_1A_1x - F_1Bw)) \\ &= \begin{bmatrix} A_gx_g - B_{gv}x_h \\ \omega_hC_gx_g \end{bmatrix} + \begin{bmatrix} B_{gw}w \\ 0 \end{bmatrix} + \\ &\begin{bmatrix} 0 \\ k_hC_gA_gx_g - \omega_hC_gx_g + k_hC_gB_{gv}x_h + k_hC_gB_{gw}w \end{bmatrix}. \end{aligned}$$

As a result of Assumption 3.1, this simplifies to

$$\dot{x} = \begin{bmatrix} A_gx_g - B_{gv}x_h \\ k_hC_gA_gx_g \end{bmatrix} + \begin{bmatrix} B_{gw}w \\ 0 \end{bmatrix}, \tag{17}$$

and thus for (16) we have

$$\left[\begin{array}{c|c} A_2 & B \\ \hline C & \end{array}\right] = \left[\begin{array}{cc|c} A_g & -B_{gv} & B_{gw} \\ k_hC_gA_g & 0 & 0_{1\times n_w} \\ \hline C_g & 0 & \\ 0_{1\times n_g} & 1 & \end{array}\right]. \tag{18}$$

Hence, (16) with (7) and (18) is an explicit PWL formulation of the HIGS controlled system in Fig. 1.

Remark 3.3. As observed from the expressions of $\mathcal{S}_1$ and $\mathcal{S}_2$ the switching in (16) is based on

$$F_2x, \ F_1x, \ \text{and } F_1(A_1x),$$

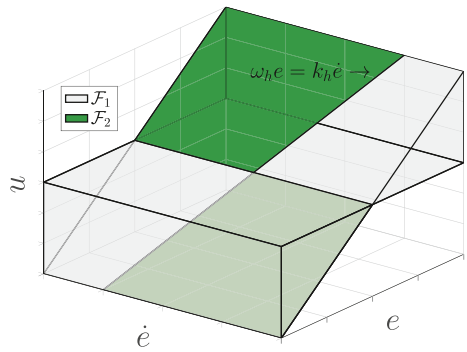

Fig. 3. Regions $\mathcal{F}_1$ and $\mathcal{F}_2$ in $(\dot{e}, e, u)$-space.

where $F_2 x = x_h = u$ is the output of the HIGS element (input u to the linear system $\mathscr{G}$ in Fig. 1) and $F_1 x = -k_h C_g x_g - x_h = -k_h e - u$, which is a function of e (output of the linear plant) and u (output of $\mathscr{H}$). Lastly, $F_1(A_1 x) = k_h \dot{e} - \omega_h e$ is a function of $\dot{e}$, the first derivative of the plant output, and the plant output e. Hence, the regions $\mathcal{S}_1$ and $\mathcal{S}_2$ can be fully described in terms of $e, \dot{e}$ and u. Indeed, one has $x \in \mathcal{S}_2$ when $(\dot{e}, e, u) \in \mathcal{F}_2$, where

$$\mathcal{F}_2 = \Big\{ (\dot{e}, e, u) \in \mathbb{R}^3 \mid (e, u) \in \mathcal{F} \wedge \\ u = k_h e \wedge w_h e^2 > k_h \dot{e} e \Big\}, \tag{19}$$

where $\mathcal{F}$ is as defined in (3). Moreover, $x \in \mathcal{S}_1$ when $(\dot{e}, e, u) \in \mathcal{F}_1$ with

$$\mathcal{F}_1 = \{(\dot{e}, e, u) \in \mathbb{R}^3 \mid (e, u) \in \mathcal{F}\} \setminus \mathcal{F}_2. \tag{20}$$

A graphical illustration of the regions $\mathcal{F}_1$ and $\mathcal{F}_2$ is provided in Fig. 3. As a result, an (internally) equivalent representation of (16) is given by

$$\Sigma : \begin{cases} \dot{x} = A_q x + B w, & \text{if } z \in \mathcal{F}_q,\ q = 1, 2, \quad \text{(i)} \\ z = \tilde{C} x, & \text{(ii)} \end{cases} \tag{21a}$$

with augmented output signal $z = [\dot{e} \quad e \quad u]^\top \in \mathbb{R}^3$, and

$$\left[\begin{array}{c|c} A_q & B \\ \hline \tilde{C} & \end{array}\right] = \left[\begin{array}{cc|c} A_g & -B_{gv} & B_{gw} \\ \tilde{B}_{h,q}\tilde{C}_g & 0 & 0_{1\times n_w} \\ \hline \tilde{C}_g & 0_{2\times 1} & \\ 0_{1\times n_g} & 1 & \end{array}\right], \tag{21b}$$

with matrices $\tilde{B}_{h,1} = [0 \quad \omega_h]$, $\tilde{B}_{h,2} = [k_h \quad 0]$, and $\tilde{C}_g = \left[(C_g A_g)^\top \quad C_g^\top\right]^\top$. We will use (9), (16), and (21) interchangeably.

From (16), we also see that we are dealing with a *discontinuous* differential equation, which makes proving (global) existence of solutions, given an initial state x_0 and external signal w, a difficult problem, since typical continuity properties used for studying differential equations/inclusions (such as upper-semicontinuity of the right-hand side cf. Aubin & Cellina, 1984) are not fulfilled, see also Cortes (2008).

4. Well-posedness analysis

In this section we show that the HIGS-controlled system (16) is well-posed in the sense of global existence of solutions. To this end, we first prove in Section 4.1 that (16) is locally well-posed, i.e., for each initial state $x(0) \in \mathcal{S}$ and exogenous signal of interest w, the system admits a solution on $[0, \epsilon]$ for some $\epsilon > 0$. We select here the class of exogenous signals (disturbances, references, etc.) to be of piecewise Bohl (*PB*) nature (see Definition 2.2). Note that sines, cosines, exponentials, polynomials, and their sums are all Bohl functions, thereby showing that the class of *PB* functions is sufficiently rich to accurately describe (deterministic) disturbances frequently encountered in practice. In particular, any piecewise constant signal is *PB*, and thus this class of functions can approximate any measurable function arbitrarily closely.[1] Building on the local existence results of Section 4.1, in Section 4.2 we prove that all (maximal) solutions are forward complete, i.e., are defined for all times $t \in \mathbb{R}_{\geq 0}$. To make this discussion precise, we will formalize the solution concept.

Definition 4.1. Let $\mathbb{T} \subset \mathbb{R}_{\geq 0}$ be an interval of the form $[0, T]$ or $[0, T)$ with $T \in \mathbb{R}_{\geq 0}$ a finite number, or $\mathbb{T} = \mathbb{R}_{\geq 0}$. A locally AC function $x : \mathbb{T} \to \mathbb{R}^n$ is called a solution to the HIGS-controlled system (16) on $\mathbb{T}$ with initial state $x_0 \in \mathcal{S}$ and $w \in PB$, if $x(0) = x_0$, $x(t) \in \mathcal{S}$ for all $t \in \mathbb{T}$, and (16) holds almost everywhere in $\mathbb{T}$.

The solutions in Definition 4.1 are *Carathéodory*-type solutions, see also Cortes (2008) for more details regarding solution concepts for discontinuous dynamical systems.

4.1. Local well-posedness

Definition 4.2. We call the HIGS-controlled system (16) locally well-posed if for all $x_0 \in \mathcal{S}$ and $w \in PB$, there exists an $\epsilon > 0$ such that the system admits a solution on $[0, \epsilon]$ with initial state x_0 and input w.

Theorem 4.1. *The HIGS-controlled system (16) is locally well-posed.*

Proof. Take $x_0 \in \mathcal{S}$ and $w \in PB$. Without loss of generality we can take $w \in B_{[0,\tilde{\epsilon}]}$ by selecting $\tilde{\epsilon} > 0$ sufficiently small. Hence, w can be represented as

$$w(t) = H_w e^{F_w t} v_w, \quad t \in [0, \tilde{\epsilon}], \tag{22}$$

for some matrices $H_w \in \mathbb{R}^{n_w \times n_{F_w}}$, $F_w \in \mathbb{R}^{n_{F_w} \times n_{F_w}}$ and a vector $v_w \in \mathbb{R}^{n_{F_w}}$. In other words, w is generated (on $[0, \tilde{\epsilon}]$) by the exo-system

$$\dot{x}_w = F_w x_w, \quad w = H_w x_w \quad x_w(0) = v_w, \tag{23}$$

Combining this exo-system with (16) yields

$$\dot{\hat{x}} = \Pi_{\hat{\mathcal{S}},\hat{E}}(\hat{x}, \hat{A}_1 \hat{x}) = \begin{cases} \hat{A}_1 \hat{x}, & \text{if } \hat{x} \in \hat{\mathcal{S}}_1, \\ \hat{A}_2 \hat{x}, & \text{if } \hat{x} \in \hat{\mathcal{S}}_2, \end{cases} \tag{24}$$
$$z = \hat{C}\hat{x},$$

where $\hat{x} = \left[x^\top \quad x_w^\top\right]^\top$ and

$$\hat{A}_1 = \begin{bmatrix} A_1 & BH_w \\ 0 & F_w \end{bmatrix}, \quad \hat{A}_2 = \begin{bmatrix} A_2 & BH_w \\ 0 & F_w \end{bmatrix}, \quad \hat{C} = \begin{bmatrix} C & 0 \end{bmatrix},$$

as an equivalent description of (16) with w as in (22) on $[0, \tilde{\epsilon}]$. Here, $\hat{E} = \left[E^\top \quad 0^\top\right]^\top$, and $\hat{\mathcal{S}} = \hat{\mathcal{K}} \cup -\hat{\mathcal{K}}$ with $\hat{\mathcal{K}} = \{\hat{x} \in \mathbb{R}^{n+n_{F_w}} \mid \hat{F}\hat{x} \geq 0\}$, where $\hat{F} = \left[\hat{F}_1^\top \quad \hat{F}_2^\top\right]^\top$ with $\hat{F}_1 = [F_1 \quad 0]$ and $\hat{F}_2 = [F_2 \quad 0]$. Furthermore, the regions $\hat{\mathcal{S}}_1$ and $\hat{\mathcal{S}}_2$ are given by

$$\hat{\mathcal{S}}_1 = \{\hat{x} \in \mathbb{R}^{n+n_{F_w}} \mid \hat{F}_2\hat{x} \geq 0 \wedge (\hat{F}_1\hat{x}, \hat{F}_1(\hat{A}_1\hat{x})) \geq_l 0\} \cup \\ \{\hat{x} \in \mathbb{R}^{n+n_{F_w}} \mid \hat{F}_2\hat{x} \leq 0 \wedge (\hat{F}_1\hat{x}, \hat{F}_1(\hat{A}_1\hat{x})) \leq_l 0\},$$
$$\hat{\mathcal{S}}_2 = \{\hat{x} \in \hat{\mathcal{S}} \mid \hat{F}_2\hat{x} \geq 0 \wedge \hat{F}_1\hat{x} = 0 \wedge \hat{F}_1(\hat{A}_1\hat{x}) < 0\} \cup \\ \{\hat{x} \in \hat{\mathcal{S}} \mid \hat{F}_2\hat{x} \leq 0 \wedge \hat{F}_1\hat{x} = 0 \wedge \hat{F}_1(\hat{A}_1\hat{x}) > 0\}.$$

[1] An interesting future research direction is establishing the existence of solutions for larger classes of input signals.

For proving local well-posedness of (24) (and thus of (16) with w as in (22)), we define the set

$$\hat{\mathcal{S}}_{\text{int}} := \{\hat{x}_0 \in \hat{\mathcal{S}} \mid \exists \epsilon > 0,\ \forall t \in [0, \epsilon],\ e^{\hat{A}_1 t}\hat{x}_0 \in \hat{\mathcal{S}}\}. \tag{25}$$

In fact, since $\hat{\mathcal{S}}_{\text{int}} \subseteq \hat{\mathcal{S}}_1$, we conclude that $e^{\hat{A}_1 t}\hat{x}_0$ is also a solution to (24) on a non-trivial time window $[0, \varepsilon]$ for some $0 < \varepsilon \leq \bar{\varepsilon}$. Next, we will also show that for each $\hat{x}_0 \in \hat{\mathcal{S}} \setminus \hat{\mathcal{S}}_{\text{int}}$, a local solution to (24) exists, so that it is established that for all $\hat{x}_0 \in \hat{\mathcal{S}}$ a local solution exists. In order to do so, we first rewrite (25) in a more algebraic form. Using the definition of $\hat{\mathcal{S}}$, one can rewrite (25) as

$$\begin{aligned}&\hat{\mathcal{S}}_{\text{int}} = \\ &\{\hat{x}_0 \mid \exists \epsilon > 0,\ \forall t \in [0, \epsilon),\ \hat{F}_1 e^{\hat{A}_1 t}\hat{x}_0 \geq 0 \wedge \hat{F}_2 e^{\hat{A}_1 t}\hat{x}_0 \geq 0\} \cup \\ &\{\hat{x}_0 \mid \exists \epsilon > 0,\ \forall t \in [0, \epsilon),\ \hat{F}_1 e^{\hat{A}_1 t}\hat{x}_0 \leq 0 \wedge \hat{F}_2 e^{\hat{A}_1 t}\hat{x}_0 \leq 0\}.\end{aligned}$$

By using the Taylor series expansion of $e^{\hat{A}_1 t}$ together with the Cayley–Hamilton theorem, the characterization $\hat{\mathcal{S}}_{\text{int}} = \hat{\mathcal{S}}^+_{\text{int}} \cup -\hat{\mathcal{S}}^+_{\text{int}}$ is obtained with

$$\begin{aligned}&\hat{\mathcal{S}}^+_{\text{int}} = \\ &\Big\{ \hat{x} \in \mathbb{R}^{n+n_{F_w}} \mid \left(\hat{F}_1\hat{x}, \hat{F}_1\hat{A}_1\hat{x}, \dots, \hat{F}_1\hat{A}_1^{n+n_{F_w}-1}\hat{x}\right) \geq_l 0 \\ &\qquad \wedge \left(\hat{F}_2\hat{x}, \hat{F}_2\hat{A}_1\hat{x}, \dots, \hat{F}_2\hat{A}_1^{n+n_{F_w}-1}\hat{x}\right) \geq_l 0 \Big\},\end{aligned}$$

Claim: $\hat{x}_0 \in \hat{\mathcal{S}} \setminus \hat{\mathcal{S}}_{\text{int}}$ implies that $\hat{F}_1\hat{x}_0 = 0 \wedge \hat{F}_2\hat{x}_0 \neq 0$. To prove the claim, note that when $\hat{x}_0$ lies in the interior of $\hat{\mathcal{S}}$, then $\hat{x}_0 \in \hat{\mathcal{S}}_{\text{int}}$ since $(\hat{F}_1\hat{x}_0 > 0 \wedge \hat{F}_2\hat{x}_0 > 0)$ or $(\hat{F}_1\hat{x}_0 < 0 \wedge \hat{F}_2\hat{x}_0 < 0)$. Moreover, $\hat{F}_2\hat{x}_0 = 0$ and $\hat{x}_0 \in \hat{\mathcal{S}}$ also imply $\hat{x}_0 \in \hat{\mathcal{S}}_{\text{int}}$. To show this, we use

$$\hat{F}_2\hat{A}_1 = \frac{\omega_h}{k_h}(\hat{F}_1 + \hat{F}_2), \tag{26}$$

which can be verified based on the expressions of $\hat{F}_2$, $\hat{A}_1$, and $\hat{F}_1$. Consider the sequence $(\hat{F}_1\hat{x}_0, \hat{F}_1\hat{A}_1\hat{x}_0, \hat{F}_1\hat{A}_1^2\hat{x}_0, \dots)$ and let $\hat{F}_1\hat{A}_1^\rho\hat{x}_0$ be the first nonzero element of the sequence for $\rho \in \mathbb{N}$. Then, it follows from (26) that $\hat{F}_2\hat{A}_1^k\hat{x}_0 = 0$ for $k = 0, 1, \dots, \rho$, and $\hat{F}_2\hat{A}_1^{\rho+1}\hat{x}_0 = \frac{\omega_h}{k_h}\hat{F}_1\hat{A}_1^\rho\hat{x}_0$. This shows that if $\hat{F}_2\hat{x}_0 = 0$ and $\hat{x}_0 \in \hat{\mathcal{S}}$, then $\hat{x}_0 \in \hat{\mathcal{S}}_{\text{int}}$ (using the lexicographic inequalities in $\hat{\mathcal{S}}^+_{\text{int}}$ and $(-\hat{\mathcal{S}}^+_{\text{int}})$). This proves the claim.

Additionally, let us make the observation that if for some $\hat{x} \in \mathbb{R}^{n+n_w}$ and some $N \in \mathbb{N}$ one has $\hat{F}_1\hat{A}_1^k\hat{x} = 0$, $k = 0, 1, 2, \dots, N$, then

$$\hat{F}_1\hat{A}_1\hat{A}_2^k\hat{x} = 0, \qquad k = 0, 1, 2, \dots, N-1, \tag{27}$$

$$\hat{F}_1\hat{A}_1\hat{A}_2^N\hat{x} = \hat{F}_1\hat{A}_1^{N+1}\hat{x}. \tag{28}$$

This identity can be easily verified by substituting the expression (15) for $\hat{A}_2$ in (27) and (28).

In case $\hat{x}_0 \in \hat{\mathcal{S}} \setminus \hat{\mathcal{S}}_{\text{int}}$, and thus $\hat{F}_1\hat{x}_0 = 0$ and $\hat{F}_2\hat{x}_0 \neq 0$, we will show that a solution of the form $\bar{x}(t) = e^{\hat{A}_2 t}\hat{x}_0 \in \hat{\mathcal{S}}_2$ exists and is a local solution to (24). For the case where $\hat{F}_2\hat{x}_0 > 0$, to show $\bar{x}(t) \in \hat{\mathcal{S}}_2$, let us note that since $\hat{F}_2\hat{x}_0 > 0$, the constraint $\hat{F}_2\bar{x}(t) \geq 0$ is satisfied by continuity for $t \in (0, \epsilon]$, with $\epsilon > 0$ sufficiently small. Thus it is sufficient to show that

$$\hat{F}_1\bar{x}(t) = 0 \wedge \hat{F}_1\hat{A}_1\bar{x}(t) < 0, \quad t \in (0, \epsilon],$$

due to the definition of $\hat{\mathcal{S}}_2$. Since we know that $\hat{F}_1\bar{x}(t) = 0$ for all t, it suffices to show that

$$\hat{F}_1\hat{A}_1\bar{x}(t) < 0, \ \text{ for } t \in (0, \epsilon]. \tag{29}$$

To prove this, we use the fact that $\hat{x}_0 \in \hat{\mathcal{S}} \setminus \hat{\mathcal{S}}_{\text{int}}$ implies

$$(\hat{F}_1\hat{A}_1\hat{x}_0, \hat{F}_1\hat{A}_1^2\hat{x}_0, \dots, \hat{F}_1\hat{A}_1^{n+n_{F_w}}\hat{x}_0) <_l 0. \tag{30}$$

By using (27) and (28), (30) implies

$$(\hat{F}_1\hat{A}_1\hat{x}_0, \hat{F}_1\hat{A}_1\hat{A}_2\hat{x}_0, \dots, \hat{F}_1\hat{A}_1\hat{A}_2^{n+n_{F_w}-1}\hat{x}_0) <_l 0, \tag{31}$$

which indeed implies (29) for some $\epsilon > 0$, and thus

$$\bar{x}(t) = e^{\hat{A}_2 t}\hat{x}_0 \in \hat{\mathcal{S}}_2 \text{ for } t \in (0, \epsilon],$$

for some $\epsilon > 0$. Therefore, $\bar{x}(t)$ is a solution to (24). As a result of the symmetry property shown in Remark 3.2, this also proves local existence of solutions when $\hat{F}_2\hat{x}_0 < 0$. Hence, we conclude local well-posedness. □

4.2. Forward completeness

Definition 4.3. Let $\mathbb{T} \subset \mathbb{R}_{\geq 0}$ be an interval of the form $[0, T]$ or $[0, T)$ with $T \in \mathbb{R}_{\geq 0}$ a finite number, or $\mathbb{T} = \mathbb{R}_{\geq 0}$. A solution $x : \mathbb{T} \to \mathbb{R}^n$ to (16) with $w \in PB$ on $\mathbb{T}$ is called maximal, if there does not exist a solution $x' : \mathbb{T}' \to \mathbb{R}^n$ with $w \in PB$ on $\mathbb{T}'$, where $\mathbb{T}' = [0, T')$ with $T' \in \mathbb{R}_{\geq T}$, that satisfies $x(t) = x'(t)$ for $t \in \mathbb{T}$. A solution $x : \mathbb{T} \to \mathbb{R}^n$ is forward complete, if $\mathbb{T} = \mathbb{R}_{\geq 0}$.

Hence, a maximal solution is a solution that cannot be prolonged (is not a strict prefix of another "larger" solution for the same input).

Theorem 4.2. *All maximal solutions to HIGS-controlled system (16) for $w \in PB$ are forward complete.*

Proof. Consider a maximal solution $x : \mathbb{T} \to \mathbb{R}^n$ of (16) for initial state $x_0 \in \mathcal{S}$ and $w \in PB$. We will show that if $\mathbb{T}$ is equal to $[0, T]$ or $[0, T)$ with $T \in \mathbb{R}_{\geq 0}$ a finite number, the left-limit $x(T) := \lim_{t \uparrow T} x(t) \in \mathcal{S}$ exists, and we can exploit the local existence result to prolong x to a solution on $[0, T + \varepsilon)$. This would contradict the maximality of the solution and thus $\mathbb{T} = \mathbb{R}_{\geq 0}$, hence x has to be forward complete.

To show the existence of $\lim_{t \uparrow T} x(t)$, let us remark that if $\mathbb{T}$ is equal to $[0, T]$, the solution is AC on $[0, T]$ and thus the left-limit trivially exists. So, the exciting case to handle is $[0, T)$. By Definition 2.2, w can be represented on $[t_i, T]$ as in (22) for some $t_i < T$ (in fact, t_i is the largest value in the set $\{t_k\}_{k \in \mathbb{N}}$, which is strictly smaller than T). Thus, (16) can be equivalently written as (24) on $[t_i, T]$. This implies the existence of a constant $M \in \mathbb{R}$ such that the vector field of (24) satisfies the linear growth condition

$$\|\Pi_{\hat{\mathcal{S}}, \hat{E}}(\hat{x}, \hat{A}_1\hat{x})\| \leq M\|\hat{x}\|, \ \text{ for all } \hat{x} \in \mathbb{R}^{n+n_{F_w}}, \tag{32}$$

because $\Pi_{\hat{\mathcal{S}}, \hat{E}}(\hat{x}, \hat{A}_1\hat{x}) \in \{\hat{A}_1\hat{x}, \hat{A}_2\hat{x}\}$. As a result of (32),

$$\begin{aligned}\|\hat{x}(t)\| &\leq \|\hat{x}_0\| + \int_0^t \|\Pi_{\hat{\mathcal{S}}, \hat{E}}(\hat{x}(\tau), \hat{A}_1\hat{x}(\tau))\| d\tau \\ &\leq \|\hat{x}_0\| + M\int_0^t \|\hat{x}(\tau)\| d\tau, \qquad \text{for } t \in [t_i, T].\end{aligned}$$

By applying Gronwall's Lemma (Khalil, 2002), one concludes that $\|\hat{x}(t)\| \leq L$ for some constant $L > 0$ and $t \in [0, T)$. Moreover, for $t \in [t_i, T]$ one has

$$\|\hat{x}(s) - \hat{x}(t)\| \leq \int_t^s \|\Pi_{\hat{\mathcal{S}}, \hat{E}}(\hat{x}(\tau), \hat{A}_1\hat{x}(\tau))\| d\tau.$$

Once again we use (32) together with $\|\hat{x}(t)\| \leq L$ to conclude $\|\hat{x}(s) - \hat{x}(t)\| \leq M\int_t^s \|\hat{x}(\tau)\| d\tau \leq ML(s - t)$. Hence, the solution $\hat{x}(t)$ is Lipschitz continuous on $t \in [t_i, T]$, and thus also absolutely continuous and uniformly continuous. Thereby, the limit $\hat{x}(T) := \lim_{t \uparrow T} \hat{x}(t)$ exists, as required. □

Since we proved local existence of solutions and forward completeness of all maximal solutions, it is concluded that for each initial state $x_0 \in \mathcal{S}$ and $w \in PB$ a global solution exists on $[0, \infty)$ and all solutions can be extended to be defined on $[0, \infty)$.

5. Time-domain stability analysis

In this section, we present a Lyapunov-based stability analysis for HIGS-controlled systems. In particular, an input-to-state stability (ISS) condition in terms of LMIs is proposed that guarantees the existence of a PWQ Lyapunov function (Johansson & Rantzer, 1998), in which a novel partitioning is used to reduce conservativeness.

Definition 5.1 ([2] *Khalil, 2002*). The closed-loop system (16) is said to be input-to-state stable (ISS), if there exist a $\mathcal{KL}$-function β and a $\mathcal{K}$-function γ such that for any initial state $x(0) \in S$ and any bounded $w \in PB$, any corresponding solution $x : \mathbb{R}_{\geq 0} \to \mathbb{R}^n$ satisfies for all $t \in \mathbb{R}_{\geq 0}$

$$\|x(t)\| \leq \beta\left(\|x(0)\|, t\right) + \gamma\left(\sup_{0\leq\tau\leq t} \|w(\tau)\|\right). \tag{33}$$

5.1. Three-dimensional partitioning

For the system given by (16) (or equivalently (21)), numerically tractable stability conditions can be formulated using LMIs. A piecewise quadratic Lyapunov function (Johansson & Rantzer, 1998) is pursued inspired by Aangenent et al. (2009) and Zaccarian et al. (2005, 2011) for reset control systems. In the cited works, however, the flow set is partitioned only in the input–output plane of the reset element, as its nonlinear behavior is captured within this two-dimensional space. As explained in Remark 3.3, the HIGS' switching dynamics, by contrast, are determined in the $(\dot{e}, e, u)$-space, requiring a novel three-dimensional partitioning to reduce conservativeness. To ensure a partitioning of the $(\dot{e}, e, u)$-space such that the edges of (some of) the resulting regions exactly coincide with the boundaries of regions where different modes are active, first note that all boundaries of the regions $\mathcal{F}_1$ and $\mathcal{F}_2$ pass through the origin (see Remark 3.3 for analytic expressions of $\mathcal{F}_1$ and $\mathcal{F}_2$). Hence, a spherical coordinate system in the $(\dot{e}, e, u)$-space can be used to realize such a partitioning. That is, the azimuthal angle θ and polar angle ϕ can be used to divide this space into polyhedral (double) cones, see $\mathcal{C}_{ij}$ in Fig. 4(a), which will be used to partition $\mathcal{F}_1$, the region where the integrator mode is active. For $\mathcal{F}_2$ (the region where the gain mode is active), which is a subset of the plane $u = k_h e$, a partitioning using the spherical coordinate system is possible using ϕ (and fixed θ), yielding regions such as depicted by $\mathcal{T}_j$ in Fig. 4(b).

The construction of the $N \times M$ polyhedral cells is as follows. Define the $N+1$ azimuthal angles and the $M+1$ polar angles

$$0 = \theta_0 < \theta_1 < \cdots < \theta_N = \arctan(k_h), \tag{34a}$$

$$0 = \phi_0 < \cdots < \phi_{M_1} < \cdots < \phi_M = \pi, \tag{34b}$$

where $\phi_{M_1} = \arctan(k_h/(\omega_h \cos(\theta_N)))$. The angle θ_N is chosen specifically such that it describes the sector boundary $u = k_h e$. Similarly, the angle ϕ_{M_1} is defined such that the vector at angular coordinates (θ_N, ϕ_{M_1}) (red vector in Fig. 4(b)) coincides with the dynamics switching boundary at the intersection of the planes $\omega_h e = k_h \dot{e}$ and the plane $u = k_h e$, at which the HIGS switches back from gain mode to integrator mode.

Let the subsets $\mathcal{C}_{ij}$ and $\mathcal{T}_j$, depicted in Fig. 4, that partition the regions where HIGS' integrator mode and gain mode are active, respectively, be given by

$$\mathcal{C}_{ij} = \{z \in \mathbb{R}^3 \mid C_{ij} z \geq 0 \ \vee \ C_{ij} z \leq 0\}, \tag{35a}$$

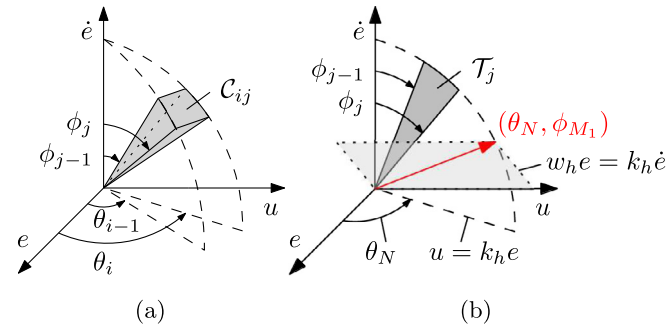

Fig. 4. In (a), one half of the (i, j)-th double-conical polyhedral region $\mathcal{C}_{ij}$ with infinite radius obtained by angular division of the spherical coordinates θ and ϕ. In (b), one half of the jth double-conical polygonal region $\mathcal{T}_j$ with infinite radius obtained by angular division in ϕ-direction on the plane $u = k_h e$ (at θ_N). The vector at angles (θ_N, ϕ_{M_1}) spanning the intersection of the planes $u = k_h e$ and $\omega_h e = k_h \dot{e}$ is shown in red. (For interpretation of the references to color in this figure legend, the reader is referred to the web version of this article.)

$$\mathcal{T}_j = \{z \in \mathbb{R}^3 \mid T_j z = [0, \alpha, \beta]^\top \ \wedge \ \alpha\beta \geq 0\}, \tag{35b}$$

where the inequalities in (35a) hold element-wise, and

$$C_{ij} = \begin{bmatrix} \Theta_{i-1} \\ -\Theta_i \\ -\Phi_{i(j-1)} \\ \Phi_{ij} \end{bmatrix}, \quad T_j = \begin{bmatrix} \Theta_N \\ -\Phi_{N(j-1)} \\ \Phi_{Nj} \end{bmatrix}. \tag{36}$$

These matrices follow from the patching hyperplanes described by $\Theta_i z = 0$ and $\Phi_{ij} z = 0$ with

$$\Theta_i = \begin{bmatrix} 0 & -\sin(\theta_i) & \cos(\theta_i) \end{bmatrix}, \tag{37a}$$

$$\Phi_{ij}^\top = \begin{bmatrix} \sin(\phi_j)\sin(\theta_i - \theta_{i-1}) \\ \cos(\phi_j)(\sin(\theta_{i-1}) - \sin(\theta_i)) \\ -\cos(\phi_j)(\cos(\theta_{i-1}) - \cos(\theta_i)) \end{bmatrix}, \tag{37b}$$

where the latter is obtained by computing the cross product of the unit vectors with angular coordinates (θ_{i-1}, ϕ_j) and (θ_i, ϕ_j), i.e., the two unit vectors that individually span the two region corners (successive in θ-direction) shared by the regions $\mathcal{C}_{ij}$ and $\mathcal{C}_{i(j+1)}$, and together spanning the common boundary plane between these regions. Note that as a result of the symmetry of the system with respect to the origin of the $(\dot{e}, e, u)$ space, the subsets $\mathcal{C}_{ij}$ as in (35a) are defined such that if $z \in \mathcal{C}_{ij}$ then $-z \in \mathcal{C}_{ij}$.

For the actual partitioning, let the index sets be defined as $\mathcal{N} = \{1, 2, \ldots, N\}$ and $\mathcal{M} = \mathcal{M}_1 \cup \mathcal{M}_2$, where $\mathcal{M}_1 = \{1, \ldots, M_1\}$ and $\mathcal{M}_2 = \{M_1 + 1, \ldots, M\}$. The closure of the integrator mode flow set $\overline{\mathcal{F}_1} = \mathcal{F}$ can then be partitioned by $\mathcal{C}_{ij}$ for $i \in \mathcal{N}, j \in \mathcal{M}$, and the gain mode flow set closure $\overline{\mathcal{F}_2} \subset \overline{\mathcal{F}_1}$ by $\mathcal{T}_j$ for $j \in \mathcal{M}_2$, i.e.,

$$\bigcup_{(i,j)\in\mathcal{N}\times\mathcal{M}} \mathcal{C}_{ij} = \overline{\mathcal{F}_1} = \mathcal{F}, \quad \bigcup_{j\in\mathcal{M}_2} \mathcal{T}_j = \overline{\mathcal{F}_2}. \tag{38}$$

Note that $\mathcal{T}_j$ captures the boundary plane of $\mathcal{C}_{Nj}$ where $u = k_h e$, hence $\mathcal{T}_j \subset \mathcal{C}_{Nj}$.

5.2. LMI-based stability condition

In addition to $\mathcal{N}$ and $\mathcal{M}$, define $\tilde{\mathcal{N}} = \mathcal{N} \backslash \{N\}$ and $\tilde{\mathcal{M}} = \mathcal{M} \backslash \{M\}$, and let $\mathbb{S}^n$ and $\mathbb{S}^n_{\geq 0}$ denote the sets of $n \times n$ symmetric matrices, the latter consisting of nonnegative elements only. The following result then states a sufficient condition for ISS of a closed-loop system with HIGS as described by (16) (or (21)).

Theorem 5.1. *If there exist matrices $U_{ij}, W_{ij} \in \mathbb{S}^4_{\geq 0}$ for $i \in \mathcal{N}, j \in \mathcal{M}$, and $V_j \in \mathbb{S}^2_{\geq 0}$ for $j \in \mathcal{M}_2$ such that $P_{ij} \in \mathbb{S}^n$ for $i \in \mathcal{N}, j \in \mathcal{M}$*

[2] A continuous function $\alpha : [0, \infty) \to [0, \infty)$ is said to belong to class $\mathcal{K}$, if it is strictly increasing and $\alpha(0) = 0$. A continuous function $\beta : [0, \infty) \times [0, \infty) \to [0, \infty)$ is said to belong to class $\mathcal{KL}$, if for each fixed s, the mapping $r \mapsto \beta(r, s)$ belongs to class $\mathcal{K}$ and, for each fixed r, the mapping $s \mapsto \beta(r, s)$ is decreasing and $\beta(r, s) \to 0$ as $s \to \infty$.

satisfy the LMIs

$$A_1^\top P_{ij} + P_{ij}A_1 + \hat{C}_{ij}^\top U_{ij}\hat{C}_{ij} \prec 0, i \in \mathcal{N}, j \in \mathcal{M}, \tag{39}$$

$$A_2^\top P_{Nj} + P_{Nj}A_2 + \hat{T}_j^\top \hat{V}_j \hat{T}_j, \prec 0, j \in \mathcal{M}_2, \tag{40}$$

$$P_{ij} - \hat{C}_{ij}^\top W_{ij}\hat{C}_{ij} \succ 0, i \in \mathcal{N}, j \in \mathcal{M}, \tag{41}$$

$$\hat{\Theta}_{i,\perp}^\top (P_{ij} - P_{(i+1)j})\hat{\Theta}_{i,\perp} = 0_{n-1}, i \in \tilde{\mathcal{N}}, j \in \mathcal{M}, \tag{42}$$

$$\hat{\Phi}_{ij,\perp}^\top (P_{ij} - P_{i(j+1)})\hat{\Phi}_{ij,\perp} = 0_{n-1}, i \in \mathcal{N}, j \in \tilde{\mathcal{M}}, \tag{43}$$

$$\hat{\Phi}_{M,\perp}^\top (P_{iM} - P_{i1})\hat{\Phi}_{M,\perp} = 0_{n-2}, i \in \mathcal{N}, \tag{44}$$

where

$$\hat{C}_{ij} = C_{ij}\tilde{C}, \quad \hat{T}_j = T_j\tilde{C}, \quad \hat{V}_j = \begin{bmatrix} v_{j,1} & v_{j,2} & v_{j,3} \\ v_{j,2} & & \\ v_{j,3} & & V_j \end{bmatrix}, \tag{45}$$

with C_{ij} and T_j from (36), arbitrary scalars $v_{j,1}, v_{j,2}, v_{j,3} \in \mathbb{R}$, $\tilde{C}$ as in (21a(i)) and where $\hat{\Theta}_{i,\perp}, \hat{\Phi}_{ij,\perp} \in \mathbb{R}^{n\times(n-1)}$ and $\hat{\Phi}_{M,\perp} \in \mathbb{R}^{n\times(n-2)}$ are matrices of full column rank such that $\mathrm{im}(\hat{\Theta}_{i,\perp}) = \ker(\Theta_i\tilde{C})$, $\mathrm{im}(\hat{\Phi}_{ij,\perp}) = \ker(\Phi_{ij}\tilde{C})$ and $\mathrm{im}(\hat{\Phi}_{M,\perp}) = \ker([0_{2\times 1} \quad I_2]\tilde{C})$, respectively, then the system in (16) (or equivalently (21)) is ISS.

Proof. Since $z = \tilde{C}x$ (21a(i)), we can define the sets

$$\hat{\mathcal{C}}_{ij} = \{x \in \mathbb{R}^n \mid \tilde{C}x = z \in \mathcal{C}_{ij}\}, \tag{46a}$$

$$\hat{\mathcal{T}}_j = \{x \in \mathbb{R}^n \mid \tilde{C}x = z \in \mathcal{T}_j\}, \tag{46b}$$

to describe the polytopic partitions in the state space of the closed-loop system. For this system, consider the radially unbounded Lyapunov function $V(x) = V_{ij}(x) = x^\top P_{ij}x$ if $x \in \hat{\mathcal{C}}_{ij}$. To prove ISS, we will show that V is an appropriate ISS Lyapunov function.

By (35a) and (46a) together with the nonnegativity of the elements in $W_{ij} \in \mathbb{S}^4_{\geq 0}$, it holds that

$$x \in \hat{\mathcal{C}}_{ij} \Rightarrow x^\top \hat{C}_{ij}^\top W_{ij}\hat{C}_{ij}x \geq 0. \tag{47}$$

As a result, using the S-procedure (41) implies that

$$V(x) = x^\top P_{ij}x > 0, \text{ if } x \in \hat{\mathcal{C}}_{ij}, \ x \neq 0, \tag{48}$$

thereby ensuring *positive definiteness* of V.

Next, using Finsler's lemma continuity of V is imposed over the boundary between two cells connected in azimuthal direction by (42) and in polar direction by (43). Since $\phi_0 = 0$ and $\phi_M = \pi$, we also require (44) to ensure continuity of V over the boundary between the first and last regions in polar direction. Note that the former two constraints ensure continuity over hyperplanes of dimension $n-1$, whereas the latter does so in only $n-2$ dimensions. This is due to the fact that in $(\dot{e}, e, u)$-space, all region boundaries are double-conical subsets of *planes*, except for the boundary *line* between the first and Mth region in ϕ-direction, i.e., on the intersection $\mathcal{C}_{i1} \cap \mathcal{C}_{iM}$. In fact, since $\phi_0 = 0$ and $\phi_M = \pi$ this boundary coincides with the $\dot{e}$-axis, i.e., at $e = u = 0$, from which it is easily seen that this leaves only $n-2$ directions in the state space of the closed-loop system in which *continuity* over this boundary must be ensured. Hence, V is a locally Lipschitz continuous function.

Inspecting the time derivative of V in integrator mode, note that due to (35a), (46a), and $U_{ij} \in \mathbb{S}^4_{\geq 0}$ it holds that

$$x \in \hat{\mathcal{C}}_{ij} \Rightarrow x^\top \hat{C}_{ij}^\top U_{ij}\hat{C}_{ij}x \geq 0, \tag{49}$$

which via the S-procedure ensures that (39) yields

$$\begin{aligned}\frac{\partial V_{ij}}{\partial x}(A_1x + Bw) &= x^\top (A_1^\top P_{ij} + P_{ij}A_1)x + 2x^\top P_{ij}Bw \\ &\leq -\varepsilon_{ij,1}\|x\|^2 + 2x^\top P_{ij}Bw,\end{aligned} \tag{50}$$

if $x \in \hat{\mathcal{C}}_{ij}$, for some $\varepsilon_{ij,1} > 0$ and $(i,j) \in \mathcal{N} \times \mathcal{M}$ by strictness of the matrix inequalities. For the gain mode, let us first observe that (35b), (46b), and $V_j \in \mathbb{S}^2_{\geq 0}$, imply

$$x \in \hat{\mathcal{T}}_j \Rightarrow x^\top \hat{T}_j^\top \hat{V}_j \hat{T}_j x \geq 0, \tag{51}$$

for $\hat{V}_j$ as in (45) with arbitrary $v_{j,1}, v_{j,2}, v_{j,3} \in \mathbb{R}$. Simultaneously employing the S-procedure and Finsler's lemma results in (40) to ensure

$$\begin{aligned}\frac{\partial V_{Nj}}{\partial x}(A_2x + Bw) &= x^\top (A_2^\top P_{Nj} + P_{Nj}A_2)x + 2x^\top P_{Nj}Bw \\ &\leq -\varepsilon_{Nj,2}\|x\|^2 + 2x^\top P_{Nj}Bw,\end{aligned} \tag{52}$$

if $x \in \hat{\mathcal{T}}_j$, with $\varepsilon_{Nj,2} > 0$ and $j \in \mathcal{M}_2$ by strictness of the LMIs in (40). Combining (50) and (52) and applying Young's inequality yields almost everywhere the upper bound on the time derivative of V over both modes

$$\dot{V} \leq -\varepsilon\|x\|^2 + \rho\|w\|^2, \tag{53}$$

with constants $\varepsilon = \min_{(i,j,q)} \varepsilon_{ij,q} - \frac{1}{\delta} > 0$ and $\rho = \delta \max_{(i,j)} \|P_{ij}B\|$, where $(i,j,q) \in \mathcal{N} \times \mathcal{M} \times \{1\}$ or $(i,j,q) \in \{N\} \times \mathcal{M}_2 \times \{2\}$ for sufficiently large $\delta > 0$. Thus, V is an appropriate PWQ ISS Lyapunov function by which the closed-loop system with HIGS is ISS. □

Remark 5.1. The constraints (42) and (43) are *sufficient* conditions for continuity of V, as they in fact demand continuity over the entire $(n-1)$-dimensional hyperplanes rather than only over the angularly bounded subset of such a hyperplane shared by two neighboring partitions. By contrast, (44) is a *necessary and sufficient* condition, requiring continuity of V only where it is truly needed. Moreover, for (44) one may remark that it would suffice to only impose this condition for any single $i \in \mathcal{N}$, provided that (42) is satisfied, since the $\dot{e}$-axis is a common boundary for all regions $\hat{\mathcal{C}}_{i1}$ and $\hat{\mathcal{C}}_{iM}$, $i \in \mathcal{N}$. In fact, the HIGS' dynamics are such that every crossing of this boundary, i.e., every zero crossing of e, leads to trajectories traveling from $\hat{\mathcal{T}}_M$ into $\hat{\mathcal{C}}_{11}$ (except for trajectories traveling through $z = 0$, for which continuity of V is already guaranteed by both (42) and (43)), and hence it would be sensible to require (44) only for $i = N$.

5.3. Discussion

The main strength of the proposed LMI-based conditions is that the discontinuous PWL dynamics are explicitly incorporated, and that the flexibility of a PWQ Lyapunov function is used to reduce conservativeness. Moreover, since the conditions pose a convex optimization problem, they can efficiently be solved by numerical algorithms. Furthermore, this LMI-based approach is general in nature in the sense that it makes no restrictive demands on $\mathcal{G}$ (only Assumption 3.1 is required), as opposed to the approach presented in Section 6, which requires stability of the linear system $\mathcal{G}$. Hence, the LMI-based approach is in principle applicable to any HIGS-controlled (motion) system that can be written in the form (16). However, being an LMI-based stability analysis, it has two aspects that might be experienced as less desirable. First, it requires an accurate parametric state–space model, which for high-precision industrial (motion) systems may not be straightforward to obtain. Second, if infeasible, the evaluated conditions provide no direction to the control engineer on how to (re)design the controller or how to guarantee robustness margins.

6. Frequency-domain conditions

In this section we discuss circle-criterion-like conditions used in Deenen et al. (2017), which similarly to the circle criterion (Khalil, 2002) exploits the sector-boundedness of the HIGS' input–output behavior to enable nonparametric stability analysis in the frequency domain.

6.1. Circle-criterion-like condition

Similar to the classical circle criterion, we inspect the frequency response function of $\mathscr{G}$ that connects the HIGS' input and output in the loop of Fig. 1, given by

$$\mathscr{G}_{ev}(s) = C_g(sI - A_g)^{-1}B_{gv}, \tag{54}$$

in relation to the HIGS' input–output sector. The following theorem states the sufficient condition for ISS.

Theorem 6.1. *Consider the system in Fig. 1 described by (16) with fixed $\omega_h \in \mathbb{R}_{>0}$ and $k_h \in \mathbb{R}_{>0}$. This system is ISS in the sense of Definition 5.1 if the following conditions are satisfied:*

(I) The system matrix A_g of (1) is Hurwitz;
(II) The transfer function $\mathscr{G}_{ev}(s)$ as in (54) satisfies

$$\frac{1}{k_h} + \Re(\mathscr{G}_{ev}(j\infty)) > 0, \qquad \text{and} \tag{55}$$

$$\frac{1}{k_h} + \Re(\mathscr{G}_{ev}(j\omega)) > 0 \text{ for all } \omega \in \mathbb{R}. \tag{56}$$

Proof. The proof is based on modifications of the circle criterion as proposed in van Loon et al. (2017). Different from van Loon et al. (2017), however, is the absence of an explicit additional detectability condition when considering the scalar-state HIGS, and the fact that, besides for the integrator dynamics, the Lyapunov function must be proven to decrease for an additional set of flow dynamics resulting from the gain mode. The proof is divided into the following steps:

(1) Initially, the internal dynamics of $\mathscr{H}$ are disregarded. Using the circle criterion, the sector-boundedness of its input–output pair (e, u) is exploited to prove ISS of $\mathscr{G}$ with respect to w by construction of a quadratic ISS Lyapunov function (Sontag, 1995) V_g via the Kalman–Yakubovich–Popov (KYP) lemma (Khalil, 2002).
(2) A quadratic Lyapunov-like function V_h is constructed for the HIGS in isolation, and an upper bound on its time derivative is found through explicit use of the sector condition and mode constraints, showing that the hybrid element is a (state) strictly passive system.
(3) The functions V_g and V_h constructed in the previous two steps are combined into a (common) quadratic ISS Lyapunov function V_c for the closed-loop system including the HIGS to prove the theorem.

Step 1: The KYP Lemma (Khalil, 2002), shows that the conditions (I) and (II) and minimality of (A_g, B_{gv}, C_g) imply the existence of a positive definite matrix $P_g \in \mathbb{S}^{n_g}$, a matrix L, and a positive constant ε_g that satisfy

$$\begin{aligned} A_g^\top P_g + P_g A_g &= -L^\top L - \varepsilon_g P_g, \\ P_g B_{gv} &= C_g^\top - \sqrt{\tfrac{2}{k_h}} L^\top. \end{aligned} \tag{57}$$

Hence, the Lyapunov function $V_g(x_g) = x_g^\top P_g x_g$ satisfies $\underline{\lambda}(P_g)\|x_g\|^2 \le V_g(x_g) \le \overline{\lambda}(P_g)\|x_g\|^2$, where $\underline{\lambda}(P_g)$ and $\overline{\lambda}(P_g)$ denote the minimum and maximum eigenvalues of the matrix $P_g \succ 0$, respectively. Following the derivation in Step 1 of the proof of Theorem 6 in van Loon et al. (2017), in which the sector condition $eu \ge \frac{1}{k_h}u^2$ from (3) is explicitly used twice, we find that the time derivative of V_g along solutions of (1) satisfies almost everywhere

$$\dot{V}_g \le -c_1\|x_g\|^2 + c_2\|w\|^2, \tag{58}$$

where $c_1 = \varepsilon_g\underline{\lambda}(P_g) - \frac{1}{\delta_1} > 0$ for sufficiently large δ_1, and $c_2 = \delta_1(\overline{\lambda}(P_g)\|B_{gw}\|)^2 > 0$, from which we conclude that V_g is indeed an ISS Lyapunov function for $\mathscr{G}$ with respect to w.

Step 2: Consider the quadratic Lyapunov function $V_h(x_h) = \frac{1}{2}c_3x_h^2$, where $c_3 = \frac{1-\delta_2}{\omega_h} > 0$ with $0 < \delta_2 < 1$, for the isolated HIGS. In integrator mode (2), the corresponding time derivative is given by

$$\dot{V}_h|_{q=1} = c_3x_h\omega_h e, \tag{59}$$

which using $u = x_h$ and the sector condition $u^2 \le k_h eu$ from (3) can be rewritten as

$$\begin{aligned} \dot{V}_h|_{q=1} &\overset{(2)}{=} -c_4x_h^2 + c_4u^2 + c_3\omega_h eu \\ &\overset{(3)}{\le} -c_4x_h^2 + (c_4k_h + c_3\omega_h)eu \\ &= -c_4x_h^2 + eu, \end{aligned} \tag{60}$$

where $c_4 = \frac{\delta_2}{k_h} > 0$ such that the last equality holds. Note that (60) shows that the integrator mode of the isolated HIGS is (state) strictly passive (Khalil, 2002). For the gain mode, let us first note that substitution of $u = k_he$ into the quadratic condition $\omega_he^2 > k_h\dot{e}e$ in (19) yields

$$\omega_h eu > k_h\dot{e}u. \tag{61}$$

We consecutively use (2), (61), and the gain mode constraint $u = k_he$ from (19) to rewrite the time derivative of V_h in gain mode as

$$\begin{aligned} \dot{V}_h|_{q=2} = c_3x_hk_h\dot{e} &\overset{(2)}{=} -c_4x_h^2 + c_4u^2 + c_3uk_h\dot{e} \\ &\overset{(61)}{<} -c_4x_h^2 + c_4u^2 + c_3\omega_h eu \\ &\overset{(19)}{=} -c_4x_h^2 + (c_4k_h + c_3\omega_h)eu, \\ &= -c_4x_h^2 + eu, \end{aligned} \tag{62}$$

which is equal to (60), and thereby denotes the uniform upper bound on $\dot{V}_h$ (almost everywhere) over both the integrator and gain mode, showing strict passivity of $\mathscr{H}$. Employing Young's inequality and $\|u\| \le k_h\|e\|$ from (3), we find almost everywhere

$$\dot{V}_h \le -c_4x_h^2 + c_5\|e\|^2, \tag{63}$$

where $c_5 = (\frac{\delta_3}{2}k_h^2 + \frac{1}{2\delta_3}) > 0$ for some $\delta_3 > 0$. Finally, substituting (1) gives almost everywhere

$$\dot{V}_h \le -c_4x_h^2 + c_6\|x_g\|^2, \tag{64}$$

where $c_6 = c_5\|C_g\|^2 > 0$.

Step 3: For the closed-loop system consisting of the interconnection of (16) (or equivalently (21)) as depicted in Fig. 1 with state $x = [x_g^\top \quad x_h]^\top$, consider the Lyapunov function

$$V_c(x_g, x_h) = V_g(x_g) + \mu V_h(x_h) = x^\top P_c x, \tag{65}$$

where $P_c = \begin{bmatrix} P_g & 0 \\ 0 & \frac{1}{2}\mu c_3 \end{bmatrix}$, and $0 < \mu < \frac{c_1}{c_6}$. V_c is positive definite and radially unbounded according to

$$\underline{\lambda}(P_c)\|x\|^2 \le V_c \le \overline{\lambda}(P_c)\|x\|^2. \tag{66}$$

An upper bound for the time derivative is given by

$$\dot{V}_c = \dot{V}_g + \mu\dot{V}_h \le -\varepsilon_c\|x\|^2 + \rho_c\|w\|^2 \tag{67}$$

almost everywhere, with $\varepsilon_c = \min(c_1 - \mu c_6, \mu c_4) > 0$ and $\rho_c = c_2 > 0$.

Consequently, we conclude that the system is ISS in the sense of Definition 5.1. □

6.2. Discussion

Condition (I) of Theorem 6.1 restricts the theorem's applicability to stable systems $\mathscr{G}$. For motion systems with floating masses, i.e., where the transfer function of the open-loop system contains poles at $s = 0$, this means that $\mathscr{G}_{ev}(s)$ may only describe an already stabilized closed-loop system. Another weakness of this approach with respect to Theorem 5.1 is the fact that this approach potentially yields a conservative estimate on stability for two main reasons. First, the Lyapunov function that underlies the circle criterion is a *common* quadratic one. Second, the actual nonlinear behavior of the HIGS is not taken into account, but instead condition (II) only considers the sector following from the HIGS gain k_h. In fact, from the Nyquist diagram of the linear system $k_h\mathscr{G}_{ev}$ we find that condition (II) directly leads to $k_{h,cc} \leq k_{h,gain}$ (which becomes an equality in case the largest negative real part of $\mathscr{G}_{ev}$ is on the real axis), where $k_{h,cc}$ denotes the smallest upper bound on the gain k_h that satisfies condition (II) of Theorem 6.1, and $k_{h,gain}$ denotes the supremum of the gain value by which the closed loop $\mathscr{G}_{ev}/(1+k_h\mathscr{G}_{ev})$ is stable. In other words, using Theorem 6.1 one can only guarantee stability for gain values k_h that also render the individual gain mode subsystem stable.

Another indication of the circle-criterion-like approach being more conservative than the LMI-based conditions is found by the inequality in (67), which implies that any Lyapunov function $V_c(x) = x^\top P_c x$ that follows from satisfying the conditions in Theorem 6.1 also satisfies the conditions (39)–(41) of Theorem 5.1 with $N = M = 1$ and $P_{11} = P_c$ (rendering the continuity constraints trivial), and with U_{11}, V_1, and W_{11} being zero matrices. Conversely, satisfying the conditions in Theorem 5.1 need not imply that the conditions in Theorem 6.1 are satisfied, hinting that the former may possibly guarantee stability in cases where the latter cannot.

The main strength of the circle-criterion-like approach lies in its convenience of application and compatibility with current industrial practice for nonparametric frequency-domain stability evaluation during the controller design process. That is, classical linear loopshaping techniques can be used to design a linear controller contained in $\mathscr{L}$ that stabilizes $\mathscr{G}_{ev}$, thereby satisfying condition (I). Also, for typical motion systems and as formalized by Assumption 3.1, it holds that $\mathscr{G}_{ev}(j\omega) \to 0$ for $\omega \to \infty$, implying (55) of condition (II) is satisfied. Thus, only (56) of condition (II) remains to be verified, which boils down to a graphical evaluation of (measured) frequency response data of $\mathscr{G}_{ev}$ with respect to the design parameter k_h in a Nyquist diagram. As such, this provides the control engineer with frequency-specific information regarding violations and robustness margins toward satisfying condition (II), which can directly be used for controller redesign.

Remark 6.1. Let us briefly elaborate on robustness issues of a discontinuous differential equation

$$\dot{x}(t) = f(x(t), w(t)), \quad \text{when } x(t) \in \mathcal{X}, \tag{68}$$

with $x(t) \in \mathbb{R}^n$, $w(t) \in \mathbb{R}^{n_w}$, and $\mathcal{X} \subseteq \mathbb{R}^n$, just as our HIGS-controlled system (9). As discussed in Goebel, Sanfelice, and Teel (2012), in order to obtain robust (with respect to arbitrary small state perturbations) stability guarantees, it is important to consider the *Krasovskii regularization* of (68), defined as

$$\dot{x}(t) \in \bigcap_{\delta>0} \mathrm{co}(f(\mathbb{B}(x(t), \delta)) \cap \mathcal{X}, w(t)), \quad \text{when } x(t) \in \overline{\mathcal{X}},$$

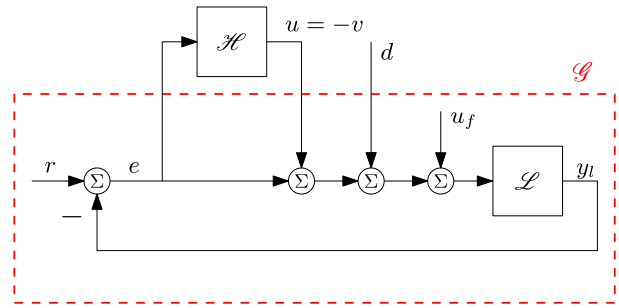

Fig. 5. A motion control feedback configuration including a HIGS, where the nonlinear HIGS $\mathscr{H}$ and the linear part $\mathscr{G}$ of the closed-loop system are indicated separately.

where $\mathbb{B}(x(t), \delta)$ is the open ball of radius δ around $x(t)$ and for a set $\Omega \subseteq \mathbb{R}^n$, $\mathrm{co}(\Omega)$ denotes its closed convex hull and $\overline{\mathcal{X}}$ denotes the closure of $\mathcal{X}$. In case of (16), its Krasovskii regularization is given as

$$\dot{x}(t) \in \begin{cases} A_1 x(t) + Bw(t), & \text{if } x(t) \in \mathcal{S}_1 \setminus \overline{\mathcal{S}_2}, \\ \mathrm{co}(A_2 x(t), A_1 x(t)) + Bw(t), & \text{if } x(t) \in \overline{\mathcal{S}_2}. \end{cases} \tag{69}$$

It can be shown that Theorems 5.1 and 6.1 hold for (69) as well, and thus stronger stability guarantees for (16) can be obtained including state perturbations (see Goebel et al., 2012 for more details).

7. Illustrative example

In this section, we demonstrate how the two stability analysis approaches of Sections 5 and 6 can be used to evaluate stability of a typical control system including a HIGS. The reader interested in time and frequency domain simulations/experiments of successful applications of HIGS-based control, is referred to Deenen et al. (2017), van den Eijnden, Heertjes, and Nijmeijer (2019) and Heertjes, van den Eijnden, Sharif, Heemels, and Nijmeijer (2019). Moreover note that in the recent work (van den Eijnden, Heertjes, Heemels, & Nijmeijer, 2020) it is shown how HIGS-based controllers overcome fundamental limitations of LTI control.

7.1. System description

Consider the SISO motion control tracking problem depicted in Fig. 5, where the LTI open-loop system $\mathscr{L}$ represents the series interconnection of a single-mass plant $\mathscr{P}$ and the stabilizing (nominal) linear controller $\mathscr{C}$ consisting of a PD-controller and first-order lowpass filter. The corresponding Laplace transforms are given by

$$\mathscr{L}(s) = \mathscr{P}(s)\mathscr{C}(s), \qquad \text{with} \tag{70a}$$

$$\mathscr{P}(s) = \frac{1}{ms^2}, \quad \mathscr{C}(s) = \frac{\omega_{lp}(k_p + k_d s)}{s + \omega_{lp}}, \tag{70b}$$

with mass $m = 1$ kg, PD-controller parameters $k_p = 1$ N/m and $k_d = 0.2$ Ns/m, and lowpass corner frequency $\omega_{lp} = 7$ rad/s, resulting in a bandwith of 1 rad/s. The plant output $y_l \in \mathbb{R}$ is the position of the mass, which must track the reference $r \in \mathbb{R}$. Using an appropriate (non-causal) feedforward signal u_f the effects of r are assumed to be fully canceled in the closed loop. As a result, the tracking error is given by $e = -y_l$, and the exogenous input $d \in \mathbb{R}$ represents only the disturbance effects. Furthermore, corresponding to Fig. 1, the linear part $\mathscr{G}$ (red dashed box) representing the baseline linear control system is in feedback with the HIGS $\mathscr{H}$, the latter generating the control

signal $u = -v \in \mathbb{R}$. In particular, the transfer function $\mathscr{G}_{ev}(s)$ is given by

$$\mathscr{G}_{ev}(s) = \frac{\mathscr{L}(s)}{1 + \mathscr{L}(s)}, \tag{71}$$

in which we recognize the complementary sensitivity function, which similarly to $\mathscr{L}(s)$ has relative degree two, thereby satisfying Assumption 3.1.

7.2. LMI-based stability analysis

Evaluation of the conditions in Theorem 5.1 requires a state–space representation of $\mathscr{G}$ as in (1). To this end, consider first the state–space model of the open-loop system $\mathscr{L}$ given by

$$\mathscr{L} : \begin{cases} \dot{x}_l = A_l x_l + B_l(e + u + d), \\ y_l = C_l x_l, \end{cases} \tag{72}$$

with states $x_l = [x_c \quad x_p^\top]^\top$ where $x_c \in \mathbb{R}$ and $x_p = [\dot{y}_l \quad y_l]^\top \in \mathbb{R}^2$ denote the controller and plant states, respectively, and corresponding matrices

$$\left[\begin{array}{c|c} A_l & B_l \\ \hline C_l & \end{array}\right] = \left[\begin{array}{ccc|c} -\omega_{lp} & 0 & 0 & k_p - k_d\omega_{lp} \\ \frac{\omega_{lp}}{m} & 0 & 0 & \frac{k_d\omega_{lp}}{m} \\ 0 & 1 & 0 & 0 \\ \hline 0 & 0 & 1 & \end{array}\right]. \tag{73}$$

To obtain a state–space description of $\mathscr{G}$ in the form of (1), we close the loop using $e = -y_l$ and $u = -v$, resulting in

$$\mathscr{G} : \begin{cases} \dot{x}_g = (A_l - B_l C_l)x_g - B_l v + B_l d, \\ e = -C_l x_g, \end{cases} \tag{74}$$

where additionally $x_g = x_l$ is substituted as no pole-zero cancellation is found to occur by closing the loop. An extended closed-loop state–space representation $\tilde{\mathscr{G}}$ follows from augmenting the output in (74) to $\tilde{e} = [\dot{e} \quad e]^\top$, which using the fact that $C_l B_l = 0$ (by Assumption 3.1) results in the matrices

$$\begin{aligned} &A_g = A_l - B_l C_l, \quad B_{gv} = -B_{gw} = -B_l, \\ &\tilde{C}_g = \begin{bmatrix} -C_l A_l \\ -C_l \end{bmatrix}, \end{aligned} \tag{75}$$

with which we can construct closed-loop system (21).

To demonstrate the added benefit of higher-dimensional partitioning of the state space, we evaluate stability using three different sets of LMI conditions:

(1) Without partitioning, which results in a common quadratic Lyapunov function. The corresponding LMIs are given by (39)–(41) for $N = M = 1$.
(2) Planar partitioning in the (e, u)-plane, yielding a two-dimensionally PWQ Lyapunov function. The evaluated LMI conditions are given by (39)–(42) for $N = 10$ and $M = 1$.
(3) Volumetric partitioning using all conditions stated in Theorem 5.1, implying the existence of a three-dimensionally PWQ Lyapunov function. For fair comparison, we choose the same number of regions $N = 10$ in the azimuthal direction as in the previous case, but now also use $M_1 = 3$ and $M_2 = 2$ to partition the state space in polar direction.

The LMI-based conditions are solved using the YALMIP toolbox (Lofberg, 2004) with SDPT3 (Tutuncu, Toh, & Todd, 2003) in MATLAB. In the implementation, the right-hand sides of (39) and (40) are tightened to $-\epsilon_1 I$, and the right-hand side of (41) is set to $\epsilon_1 I$, where $\epsilon_1 = 10^{-3}$ is sufficiently large with respect to the machine precision such that the resulting LMIs may be solved in a non-strict manner for solver compatibility. Furthermore, similar

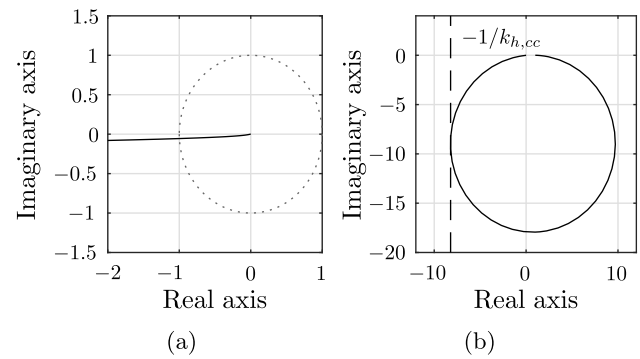

Fig. 6. Nyquist diagrams of (a) $\mathscr{L}(s)$ for evaluating stability of $\mathscr{G}(s)$, and (b) $\mathscr{G}_{ev}(s)$ against the value $-1/k_{h,cc}$.

to *Remark 4* in Zaccarian et al. (2011), the equality constraints (42)–(44) are replaced by auxiliary inequality constraints with a small tolerance of $\epsilon_2 = 10^{-8}$ to reduce numerical problems. Moreover, a balancing state transformation $\tilde{x}_g = T_g x_g$ with $T_g \in \mathbb{R}^{n_g \times n_g}$ is applied to the linear system with matrices (75) to improve numerical conditioning. Stability is evaluated using Theorem 5.1 for a grid of HIGS parameter values (k_h, ω_h), the results of which are shown in Fig. 7 and will be discussed in more detail in Section 7.4.

7.3. Frequency-domain stability analysis

To evaluate stability of the closed-loop system using the circle-criterion-like approach, we simply inspect the complementary sensitivity function (71). In verifying the conditions of Theorem 6.1, we first observe that condition (I) is satisfied by design of the nominal controller $\mathscr{C}$, as can also be seen from Fig. 6(a) using the Nyquist criterion. Next, since $\mathscr{G}_{ev}(s)$ has a relative degree of two, it holds that $\mathscr{G}_{ev}(j\omega) \to 0$ as $\omega \to \infty$, meaning (55) in condition (II) is satisfied for any $k_h > 0$. For (56) in condition (II), we inspect the Nyquist diagram of (71) shown in Fig. 6(b), from which it follows that the closed-loop system including HIGS is guaranteed to be ISS by Theorem 6.1 for any $\omega_h \in (0, \infty)$ and $k_h < k_{h,cc} = 0.12$, as indicated in Fig. 7 by the region to the left of dashed red line.

7.4. Comparison

For a grid of HIGS parameters (k_h, ω_h), Fig. 7 visualizes the range of parameter values for which the different approaches are able to guarantee closed-loop stability of the HIGS-controlled example system (70). In addition, the figure shows the parameter range for which the system has been concluded to be stable on the basis of time-series simulation studies. Fig. 7 illustrates the conservativeness associated with this frequency-based approach, which can only guarantee stability for HIGS gains up to $k_{h,cc} = 0.12$ (dashed red line). This conservativeness is thought to stem partly from inadequately accounting for the true nonlinear dynamics determined by the parameter pair (k_h, ω_h), and instead using an upper bound based only on k_h, which is evident in Fig. 7 as the stable parameter region according to Theorem 6.1 does not depend on ω_h.

The LMI-based approach without partitioning, on the contrary, does explicitly include the nonlinear closed-loop dynamics. Consequently, the corresponding range of verifiably stable parameter values (black dots) increases with respect to the circle criterion, see Fig. 7(a). Comparing to the simulation-based stable region

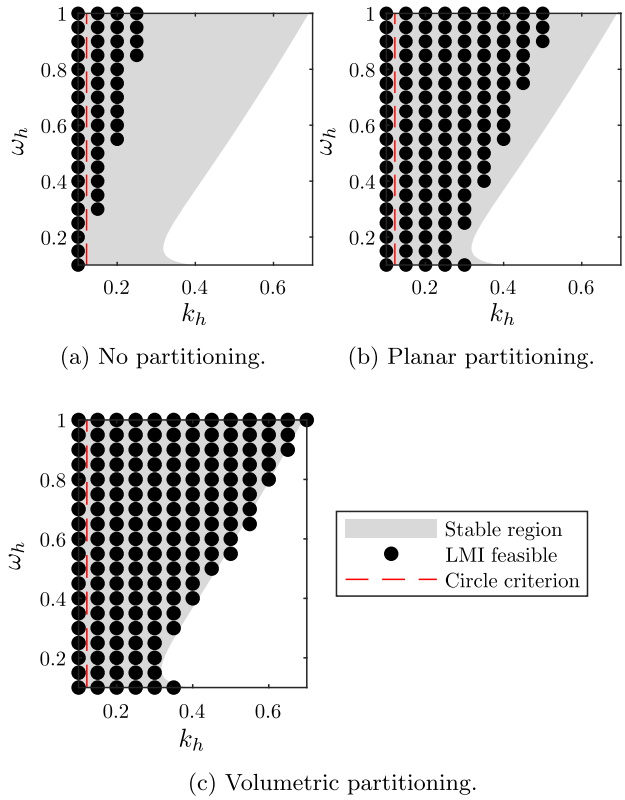

(a) No partitioning. (b) Planar partitioning.

(c) Volumetric partitioning.

Fig. 7. A comparison of the HIGS parameters (k_h, ω_h) for which stability can be guaranteed by the circle criterion (area left of dashed red line), or by the LMI-based conditions (a) without partitioning, and with (b) planar and (c) volumetric partitioning (black dots). The parameter values for which stable responses have been observed in simulation are indicated by the gray area. (For interpretation of the references to color in this figure legend, the reader is referred to the web version of this article.)

(gray), however, a considerable degree of conservativeness remains due to the LMIs demanding the existence of a common Lyapunov function. In Fig. 7(b), it is shown that the planar partitioning as described by Theorem 5.1 for $M = 1$ is able to partly alleviate this problem, resulting in a significantly larger set of parameters for which stability can be guaranteed. For parameter pairs close to the edge of the stable region, also this approach is consistently unable to guarantee stability. Finally, Fig. 7(c) illustrates the potential of the conditions in Theorem 5.1 in terms of reducing the conservativeness by extending the partitioning to three dimensions. The resulting range of (k_h, ω_h)-values for which closed-loop stability can be concluded on the basis of LMI conditions approximately coincides with the stable parameter region found by time-series simulation . Clearly, the LMI-based analysis outperforms the circle-criterion-like approach in terms of conservativeness. Nevertheless, the latter may sometimes be the preferable option due to its conditions being easier to verify. This is especially true in practice, in case accurate state–space models such as (72) are not available. The other potential drawbacks of the LMI-based approach are caused by the conditions being evaluated qualitatively, numerically, and for only a single parameter pair (k_h, ω_h) at a time. Moreover, using numerical solvers may cause sensitivity to numerical inaccuracies, especially those related to the continuity constraints (42)–(44). In particular, if ϵ_2 is chosen too small, the solver may be unable to find a feasible solution for some values (k_h, ω_h) within the stable region, while for ϵ_2 too large, increasingly many false positive conclusions on stability occur outside the stable region. Moreover, the suitable tolerance values may depend on the number of partitions N, M_1, and M_2, which in turn affects the number of LMIs and thereby the required solver time. The process of finding a suitable partitioning and corresponding tolerance values, combined with the fact that each value of the pair (k_h, ω_h) must be evaluated individually, renders this approach more time-consuming compared to the circle-criterion-like analysis.

Remark 7.1. To reduce the numerical sensitivity of the LMI-based approach in this example, we tuned the PD-controller with reduced robustness margins, allowing for a fair comparison of the conservativeness of the different approaches (i.e., independent of numerical issues).

8. Conclusion

In this paper, we have introduced the formalization of the hybrid integrator-gain system (HIGS). The HIGS is a nonlinear integrator that projects its dynamics onto a sector, thereby keeping the sign of its input and output the same while maintaining a continuous control signal. We have presented an appropriate mathematical framework for the formal description of HIGS-controlled systems based on generalizations of projected dynamical systems, called extended projected dynamical systems (ePDS), which naturally describes the main design philosophy behind the HIGS. The ePDS framework was used in showing the fundamental property of well-posedness of HIGS-controlled systems in the sense of existence and forward completeness of solutions, thereby laying down a mathematical framework for formal studies of HIGS-based controllers. Moreover, two approaches for analyzing closed-loop stability of a motion system including a HIGS have been presented. The first involves LMI-based conditions that guarantee ISS of the closed-loop system via a PWQ Lyapunov function. Its main strength lies in a novel three-dimensional partitioning of the state space specifically tailored to the HIGS' dynamics, which reduces conservativeness of the conditions to a degree similar to what would be expected from a necessary condition on closed-loop stability. The second approach involves a circle-criterion-like analysis. Although potentially more conservative and only applicable to certain (common) feedback configurations, this approach allows for a nonparametric frequency-domain evaluation of input-to-state stability of the closed-loop system including HIGS. Both methods have been demonstrated on a motion system. Since their strengths and weaknesses are largely complementary, together they form a powerful set of tools for the stability analysis of HIGS-controlled systems.

References

Aangenent, W. H. T. M., Witvoet, G., Heemels, W. P. M. H, van de Molengraft, M. J. G, & Steinbuch, M. (2009). Performance analysis of reset control systems. *International Journal of Robust and Nonlinear Control*, *20*(11), 1213–1233.

Aubin, J., & Cellina, A. (1984). *Differential inclusions: set-valued maps and viability theory*. Springer-Verlag Berlin Heidelberg New York Tokyo.

Baños, A., & Barreiro, A. (2012). *Advances in industrial control*, *Reset control systems*. London: Springer London.

Baños, Alfonso, Perez, Felix, & Cervera, Joaquin (2013). Network-based reset control systems with time-varying delays. *IEEE Transactions on Industrial Informatics*, *10*(1), 514–522.

Barreiro, A., & Baños, A. (2010). Delay-dependent stability of reset systems. *Automatica*, *46*(1), 216–221.

Beker, O., Hollot, C. V., & Chait, Y. (2001). Plant with integrator: an example of reset control overcoming limitations of linear feedback. *IEEE Transactions on Automatic Control*, *46*(11), 1797–1799.

Beker, O., Hollot, C. V., Chait, Y., & Han, H. (2004). Fundamental properties of reset control systems. *Automatica*, *40*(6), 905–915.

Boyd, S., & Vandenberghe, L. (2004). *Convex optimization*. Cambridge University Press.

Carrasco, J., & Navarro-López, E. (2013). Towards l_2-stability of discrete-time reset control systems via dissipativity theory. *Systems & Control Letters*, *62*(6), 525–530.

Chait, Y., & Hollot, C. V. (2002). On Horowitz's contributions to reset control. *International Journal of Robust and Nonlinear Control*, *12*(4), 335–355.

Clegg, J. (1958). A nonlinear integrator for servomechanisms. *Transaction of American Institute of Electrical Engineers, Part II: Applications and Industry*, *77*(1), 41–42.

Cortes, J. (2008). Discontinuous dynamical systems. *IEEE Control Systems Magazine*, *28*(3), 36–73.

Deenen, D. A., Heertjes, M. F., Heemels, W. P. M. H., & Nijmeijer, H. (2017). Hybrid integrator design for enhanced tracking in motion control. In *2017 American control conference* (pp. 2863–2868). IEEE.

Dupuis, P., & Nagurney, A. (1993). Dynamical systems and variational inequalities. *Annals of Operations Research*, *44*(1), 7–42.

van den Eijnden, S. J. A. M., Heertjes, M. F., Heemels, W. P. M. H., & Nijmeijer, H. (2020). Hybrid integrator-gain systems: A remedy for overshoot limitations in linear control? *IEEE Control Systems Letters*, *4*, 1042–1047.

Feuer, A., Goodwin, G., & Salgado, M. (1997). Potential benefits of hybrid control for linear time invariant plants. In *1997 American control conference* (pp. 2790–2794). IEEE.

Freudenberg, J., Middleton, R., & Stefanpoulou, A. (2000). A survey of inherent design limitations. In *2000 American control conference ACC* (pp. 2987–3001). IEEE.

Goebel, R., Sanfelice, R. G., & Teel, A. R. (2012). *Hybrid dynamical systems: modeling, stability, and robustness*. Princeton University Press.

Guo, Y., Wang, Y., Xie, L., & Zheng, J. (2009). Stability analysis and design of reset systems: Theory and an application. *Automatica*, *45*(2), 492–497.

Hauswirth, A., Bolognani, S., & Dorfler, F. (2021). Projected dynamical systems on irregular, non-Euclidean domains for nonlinear optimization. *SIAM Journal on Control and Optimization*, *59*(1), 635–668.

Hazeleger, L., Heertjes, M. F., & Nijmeijer, H. (2016). Second-order reset elements for stage control design. In *2016 American control conference* (pp. 2643–2648). IEEE.

Heertjes, M. F., van den Eijnden, S. J. A. M., Sharif, B., Heemels, W. P. M. H., & Nijmeijer, H. (2019). Hybrid integrator-gain system for active vibration isolation with improved transient response. *IFAC-PapersOnLine*, *52*(15), 454–459.

Henry, C. (1973). An existence theorem for a class of differential equations with multivalued right-hand side. *Journal of Mathematical Analysis and Applications*, *41*(1), 179–186.

Horowitz, I., & Rosenbaum, P. (1975). Non-linear design for cost of feedback reduction in systems with large parameter uncertainty. *International Journal of Control*, *21*(6), 977–1001.

Johansson, M., & Rantzer, A. (1998). Computation of piecewise quadratic Lyapunov functions for hybrid systems. *IEEE Transactions on Automatic Control*, *43*(4), 555–559.

Khalil, Hassan K. (2002). *Nonlinear systems* (3rd ed.). Inc Up. Saddle River, NJ.

Lofberg, J. (2004). YALMIP : a toolbox for modeling and optimization in MATLAB. In *2004 IEEE international conference on robotics and automation* (pp. 284–289).

van Loon, S. J. L. M., Gruntjens, K. G. J., Heertjes, M. F., van de Wouw, N., & Heemels, W. P. M. H. (2017). Frequency-domain tools for stability analysis of reset control systems. *Automatica*, *82*, 101–108.

Nagurney, A., & Zhang, D. (2012). *Projected dynamical systems and variational inequalities with applications*. Springer Science & Business Media.

Nešić, D., Teel, A. R., & Zaccarian, L. (2011). Stability and performance of SISO control systems with first-order reset elements. *IEEE Transactions on Automatic Control*, *56*(11), 2567–2582.

Nešić, D., Zaccarian, L., & Teel, A. R. (2008). Stability properties of reset systems. *Automatica*, *44*(8), 2019–2026.

Prieur, C., Queinnec, I., Tarbouriech, S., & Zaccarian, L. (2018). Analysis and synthesis of reset control systems. *Foundations and Trends in Systems and Control*, *6*(2–3), 117–338.

Rockafellar, R. T., & Wets, R. J. B. (1998). *Variational analysis*. Heidelberg, Berlin, New York: Springer Verlag.

Saikumar, N., & Hosseinnia, H. (2017). Generalized fractional order reset element (GFrORE). In *European nonlinear dynamics conference*.

Seron, M. M., Braslavsky, J. H., & Goodwin, G. C. (1997). *Communications and control engineering, Fundamental limitations in filtering and control* (p. 380). London: Springer-Verlag.

Sharif, B., Heertjes, M. F., & Heemels, W. P. M. H. (2019). Extended projected dynamical systems with applications to hybrid integrator-gain systems. In *2019 IEEE conference on decision and control* (pp. 5773–5778).

Sontag, E. (1981). Nonlinear regulation: The piecewise linear approach. *IEEE Transactions on Automatic Control*, *26*(2), 346–358.

Sontag, E. (1995). On the input-to-state stability property. *European Journal of Control*, *1*(1), 24–36.

Tutuncu, R. H., Toh, K. C., & Todd, M. J. (2003). Solving semidefinite-quadratic-linear programs using SDPT3. *Mathematical Programing*, *95*(2), 189–217.

van den Eijnden, S. J. A. M., Heertjes, M. F., & Nijmeijer, H. (2019). Robust stability and nonlinear loop-shaping design for hybrid integrator-gain-based control systems. In *2019 American control conference* (pp. 3063–3068). IEEE.

Vidal, A., & Banos, A. (2008). QFT-Based design of PI+ CI reset compensators: application in process control. In *2008 Mediterranean conference on control and automation* (pp. 806–811). IEEE.

Zaccarian, L., Nešić, D., & Teel, A. R. (2005). First order reset elements and the Clegg integrator revisited. In *2005 American control conference* (pp. 563–568). IEEE.

Zaccarian, L., Nešić, D., & Teel, A. R. (2011). Analytical and numerical Lyapunov functions for SISO linear control systems with first-order reset elements. *International Journal of Robust and Nonlinear Control*, *21*(10), 1134–1158.

Zhao, G., Nešić, D., Tan, Y., & Hua, C. (2019). Overcoming overshoot performance limitations of linear systems with reset control. *Automatica*, *101*, 27–35.

Zheng, Y., Chait, Y., Hollot, C. V., Steinbuch, M., & Norg, M. (2000). Experimental demonstration of reset control design. *Control Engineering Practice*, *8*(2), 113–120.

Daniel Andreas Deenen received the M.Sc. (cum laude) and Ph.D. degrees in control engineering from the Department of Mechanical Engineering at the Eindhoven University of Technology, the Netherlands, in 2016 and 2020, respectively. His Ph.D. work focused on estimation and model predictive temperature control strategies for magnetic-resonance-guided high-intensity focused ultrasound (MR-HIFU) hyperthermia in cancer treatment. In addition, his research interests include hybrid and reset control with application to high-precision industrial systems.

Bardia Sharif received the M.Sc. degree (Cum Laude) in electrical engineering with specialization in systems and control from Eindhoven University of Technology (TU/e), in 2018. Since 2018, he has been pursuing a Ph.D. degree in the Control Systems Technology Group, Department of Mechanical Engineering, TU/e. His current research interests include hybrid systems and control with particular focus on formalization, analysis and design/synthesis of hybrid control solutions aiming at realizing performance beyond limitations of linear time invariant (LTI) control.

Sebastiaan van den Eijnden was born in 1991. He received the M.Sc. degree in Mechanical Engineering from the Eindhoven University of Technology in 2017, where he is currently pursuing the Ph.D. degree within the Department of Mechanical Engineering. His current research interests include analysis and design of nonlinear/hybrid (control) systems, and advanced motion control.

Henk Nijmeijer (1955) is a full professor at Eindhoven and chairs the Dynamics and Control group. He is an editor of Communications in Nonlinear Science and Numerical Simulations. He is a fellow of the IEEE since 2000 and was awarded in 1990 the IEE Heaviside premium. He is appointed honorary knight of the golden feedback loop (NTNU, Trondheim) in 2011. Per January 2015 he is scientific director of the Dutch Institute of Systems and Control (DISC). He is recipient of the 2015 IEEE Control Systems Technology Award and a member of the Mexican Academy of Sciences. He is Graduate Program director of the TU/e Automotive Systems program. He is an IFAC Fellow since 2019 and as of January 2021 an IEEE Life Fellow.

Maurice Heemels received M.Sc. (mathematics) and Ph.D. (EE, control theory) degrees (summa cum laude) from the Eindhoven University of Technology (TU/e). Currently, Maurice is a Full Professor at ME, TU/e. He held visiting professor positions at ETH, Switzerland (2001), UCSB, USA (2008) and University of Lorraine, France (2020). He is a Fellow of the IEEE and the chair of the IFAC Technical Committee on Networked Systems. He was the recipient of the 2019 IEEE L-CSS Outstanding Paper Award and was elected for the IEEE-CSS Board of Governors (2021–2023).

Marcel Heertjes received the M.Sc. and Ph.D. degrees from the Eindhoven University of Technology, Eindhoven, The Netherlands, in 1995 and 1999, respectively. After being with the Philips Center for Industrial Technology from 2000–2005, he joined ASML in 2006. He was a recipient of the IEEE Control Systems Technology Award 2015 for variable gain control and its applications to wafer scanners. In 2019, he was appointed (part-time) full Professor on Industrial Nonlinear Control for High-Precision Systems at Eindhoven University of Technology. He acts as an Associate Editor for IFAC Mechatronics since 2016.